



Thermodynamic Properties of Liquid Toluene from Speed-of-Sound Measurements at Temperatures from 283.15 K to 473.15 K and at Pressures up to 390 MPa

Subash Dhakal¹ · Weparn J. Tay² · Saif Z. S. Al Ghafri¹ · Darren Rowland¹ · Sean P. Mullins¹ · Eric F. May¹ · J. P. Martin Trusler² · Paul L. Stanwix¹ 

Received: 20 July 2021 / Accepted: 29 August 2021 / Published online: 27 September 2021
© The Author(s), under exclusive licence to Springer Science+Business Media, LLC, part of Springer Nature 2021

Abstract

We report the speeds of sound in liquid toluene (methylbenzene) measured using double-path pulse-echo apparatus independently at The University of Western Australia (UWA) and Imperial College London (ICL). The UWA data were measured at temperatures between (306 and 423) K and at pressures up to 65 MPa with standard uncertainties of between (0.02 and 0.04)%. At ICL, measurements were made at temperatures between (283.15 and 473.15) K and at pressures up to 390 MPa with standard uncertainty of 0.06%. By means of thermodynamic integration, the measured sound-speed data were combined with initial density and isobaric heat capacity values obtained from extrapolated experimental data to derive a comprehensive set of thermodynamic properties of liquid toluene over the full measurement range. Extensive uncertainty analysis was performed by studying the response of derived properties to constant and dynamic perturbations of the sound-speed surface, as well as the initial density and heat capacity values. The relative expanded uncertainties at 95% confidence of derived density, isobaric heat capacity, isobaric expansivity, isochoric heat capacity, isothermal compressibility, isentropic compressibility, thermal pressure coefficient and internal pressure were estimated to be (0.2, 2.2, 1.0, 2.6, 0.6, 0.2, 1.0 and 2.7)%, respectively. Due to their low uncertainty, these data and derived properties should be well suited for developing a new and improved fundamental Helmholtz equation of state for toluene.

Keywords Derived thermodynamic properties · Speed of sound · Thermodynamics · Toluene · Uncertainty analysis

✉ J. P. Martin Trusler
m.trusler@imperial.ac.uk

✉ Paul L. Stanwix
paul.stanwix@uwa.edu.au

Extended author information available on the last page of the article

1 Introduction

Toluene (methylbenzene, C_7H_8) is predominantly used in the production of paints, rubbers, glues and adhesives. It is also a widely used solvent, a precursor in explosives manufacture and a component of high-octane gasolines [1]. Toluene can be obtained with high purity, has relatively low toxicity and corrosivity, and exists in the liquid state over a wide range of temperature, making it suitable as a calibration fluid in measurements of thermophysical properties such as density and viscosity [2, 3].

The use of toluene in various applications depends on the reliability of models to predict its thermodynamic properties over wide ranges of temperature and pressure. Such predictions are best made using fundamental equations of state (EOS) [4]. Several models have been developed for toluene. The most widely used is the Helmholtz EOS developed by Lemmon and Span [4], which is valid over a temperature range of (178 to 700) K and pressures up to 500 MPa. The development of equations of state for any fluid requires accurate experimental data for a range of thermodynamic properties, including the speed of sound. The speed of sound in liquid toluene has been reported by several investigators (Table 1). The distribution of the literature data in (T, p) -space is provided in Fig. 1 along with the vapour–liquid phase boundary.

It is noteworthy that the most extensive and accurate experimental campaigns were conducted after the development of the Helmholtz EOS by Lemmon and

Table 1 Summary of the literature of experimental speed-of-sound data of toluene

References	Year	N^*	Method	T (K)	p (MPa)	Uncertainty
Speed of sound at atmospheric pressure and along saturation pressure, p_s						
Freyer [5]	1929	6	SI ^a	273.15–323.15	0.1	1 m·s ⁻¹
Desphande [6]	1968	3	OI ^b	298.14–318.13	0.1	0.15%
Zotov [7]	1969	19	PE ^c	293.14–473.15	p_s	2 m·s ⁻¹
Reddy [8]	1986	8	SI	303.14–313.14	0.1	0.1%
Tamura [9]	1985	3	PE	293.15–303.15	0.1	0.1%
Gongalez-Olmos [10]	2007	15	PE	288.15–323.15	0.1	1 m·s ⁻¹
Luning Prak [11]	2014	10	PE	293.15–373.15	0.1	1 m·s ⁻¹
Dragoescu [12]	2019	6	PE	298.15–318.15	0.1	0.5 m·s ⁻¹
Speed-of-sound in compressed liquid phase						
Tagaki [13]	1985	17	PE	303.15	0.1–160	0.3%
Muringer [14]	1985	88	PE	173.18–320.30	0.1–263.45	5.1 m·s ⁻¹
Okhotin [15]	1988	150	PE	273.15–473.11	0.1–58.93	0.05%
Vervieko [16]	1991	24	PE	293–373	0.1–250	0.3%
Meier [17]	2013	222	PE	280–420	0.1–100.17	0.03%
Yebra [18]	2017	84	PE	283.15–343.15	0.1–95.1	0.1%
Shchamialiou [19]	2020	36	PE	298.15–433.15	0.1–100.1	0.1%

^aSonic interference, ^bOptical interference, ^cPulse-echo

*Number of points measured

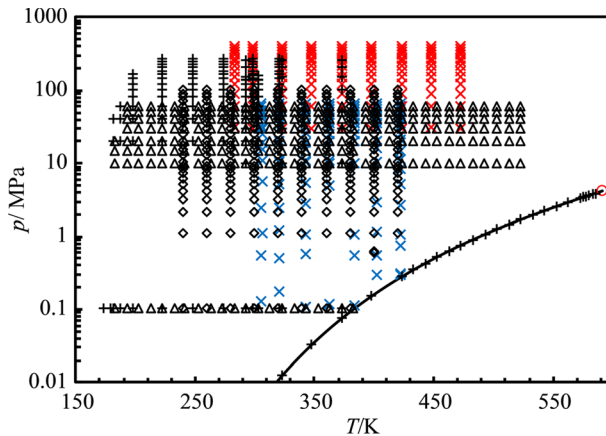


Fig. 1 Measurement conditions for selected low-uncertainty experimental data of speed-of-sound of liquid Toluene available in the literature (Table 1) and experimental data investigated in this work. \times , UWA; \times , ICL; \diamond , Meier et al. [17]; Δ , Okhotin et al. [15]; $+$, other experimental data; \circ , Critical point stated by Helmholtz EOS [4]. The solid line represents the vapour–liquid phase boundary

Span [4]. Due in part to the lack of highly accurate experimental data at the time, the uncertainties in speeds of sound predicted by the EOS (1% at pressure up to 100 MPa and temperature up to 500 K, increasing to 2% at higher values of pressure and temperature [4]) are considerably larger than the reported standard uncertainties of current data, e.g. well below 0.1% at pressures up to 100 MPa and temperatures up to 420 K [17].

In this work, we extend both the temperature and pressure ranges at which highly accurate speed-of-sound measurements in liquid toluene have been determined. Based on the measured speeds of sound, we have employed thermodynamic integration to obtain a comprehensive set of thermodynamic properties over the full range of the measurements with small uncertainties. The speeds of sound and derived properties are also compared with available literature data and predictions based on the Helmholtz EOS of Lemmon and Span [4].

2 Experimental Procedure

The sound-speed measurements were carried out using two sets of double-path pulse-echo equipment having different but overlapping operating pressure ranges. At UWA, the apparatus was the same as that used recently by Al Ghafri et al. [20] in their study of p-xylene. This apparatus uses a dual-path ultrasonic cell, mounted within a high-pressure stainless-steel vessel, with signal excitation and detection achieved with a gold-plated piezoelectric ceramic disc transducer operated at 5 MHz. The apparatus was housed in a thermostatic air bath maintaining temperature stability of better than 0.1 K. Temperature measurements were carried out using platinum resistance thermometer (PRT) probes (Netsushin model NR-141-100S, 1.6 mm diameter) with a standard uncertainty of 0.02 K.

Considering the stability of the oven, non-uniformity of temperature across the cell, and the calibration uncertainty, the standard uncertainties in temperature were estimated to be 0.03 K for $T=(306, 320 \text{ and } 343)$ K, 0.04 K for $T=(363 \text{ and } 383)$ K, 0.05 K for $T=403$ K, and 0.07 K for $T=423$ K. Pressure was measured using a pressure transmitter (Keller model PA-33X) with a full-scale reading of 70 MPa and a manufacturer-specified relative uncertainty of 0.05% ($k=1.73$). Its calibration was validated against a hydraulic pressure balance (DH-Budenberg model EHX-580, relative standard uncertainty 0.008%) and the greatest absolute deviation was found to be 0.019 MPa. Taking this into account, the standard uncertainty of pressure was estimated to be 0.02 MPa within the experimental range. The calibration of the apparatus for this study was carried out using water and has been detailed previously by Al Ghafri et al. [20].

The apparatus used at ICL employed a similar 5 MHz double-path pulse-echo apparatus housed in a stainless-steel high-pressure vessel and immersed in a thermostatic oil bath. This apparatus, described in detail by Tay and Trusler [21], had an extended operating temperature ranges of (273.15 to 473.15) K with pressures up to 390 MPa. Pressure was measured with a pressure transducer (Honeywell model TJE/60000) having an estimated standard uncertainty of 0.05 MPa or $6 \times 10^{-4} \cdot p$, whichever is greater. Temperature was measured using a PRT (Fluke Model 5615) with a standard uncertainty of 0.015 K. Calibration was carried out with water as a part of the work described earlier [21]. The toluene (methylbenzene) samples were used as supplied by Sigma-Aldrich. The sample descriptions, including batch/lot and purity analysis as provided by the supplier, are listed in Table 2 for both UWA and ICL. Other than degassing the samples, no further purification or analysis was performed.

Experimental uncertainties in the speed of sound arise from the uncertainties in the pressure, temperature, and pulse-echo time delays under both calibration and measurement conditions. Additional uncertainties are associated with the speed of sound in the calibration fluid(s) and with the thermal expansion and compressibility of the ultrasonic cell [21]. For the apparatus used at UWA, the combined standard relative uncertainty in the speed of sound was found to vary between 0.01% and 0.04%, with the greatest relative uncertainty found at the highest temperature and lowest pressure studied. For the measurements carried out at ICL, the standard relative uncertainty was found to have an almost constant value of 0.06%.

Table 2 Description of chemical samples used in the study where w is mass-fraction purity

Chemical name	CAS number	Source	Purity w	Purification	Analysis ^a
Toluene ^b	108-88-3	Sigma-Aldrich ^c	0.9993	Vacuum degassed	GC
Toluene	108-88-3	Sigma-Aldrich ^d	0.9994	Vacuum degassed	GC

^aGas-chromatography. ^bMethylbenzene. ^cBatch number: SHBG1684V, $w(\text{H}_2\text{O}) \leq 0.00001$. ^dLot number: MKBX7400V, $w(\text{H}_2\text{O}) \leq 0.00001$

3 Experimental Results

We report a total of 274 different sound-speed experimental values along with the associated uncertainties. A total of 157 sound-speed data points of toluene were measured in the liquid region along seven isotherms of average temperatures $T = (306.25, 320.42, 343.38, 363.19, 383.41, 403.07, \text{ and } 422.61)$ K at pressures up to 65 MPa at UWA. The measured speed-of-sound data with the standard uncertainties are provided in Table 3. Similarly, at ICL, a total of 117 measurements were carried out at temperatures of $(283.15, 298.15, 323.15, 348.15, 373.15, 398.15, 423.15, 448.15, \text{ and } 473.15)$ K and at pressures between (30 and 390) MPa. The measured sound-speed data along with the standard uncertainties are provided in Table 4. In both laboratories, measurements were carried out along isotherms, starting from lowest pressure. For repeatability checks, the pressure was brought back to certain selected values along the fixed isotherm. Similarly, after completing all sets of measurements along each isotherm, the temperatures were returned to selected values to check for the repeatability of the results. At UWA, measurements were also repeated at selected pressures and temperatures to check for the reproducibility of the results when fresh samples were introduced. The relative change in the initial and repeated measurements in all cases was within 0.01% which confirms that the sensor and the sample were stable during the measurements.

4 Correlation of Data

In order to facilitate comparison with the existing literature and equation-of-state predictions, the measured speed-of-sound data were combined and correlated as a function of pressure and temperature. The thermodynamic integration procedure, discussed later, also depends on the accurate correlation of the speed-of-sound data over the experimental range. The data were correlated in terms of the following equations as employed previously by Al Ghafri et al. [20]:

$$p - p_0 = \sum_{i=1}^3 \sum_{j=0}^3 a_{ij} (c - c_{0,T}) / \left(\frac{T}{T_0} \right)^j \quad (1)$$

$$c_{0,T} = \sum_{j=0}^3 b_j \left(\frac{T}{T_0} \right)^j. \quad (2)$$

Here, $p_0 = 0.1$ MPa is a reference pressure, $T_0 = 300$ K is a reference temperature, $c_{0,T}$ is the speed of sound at temperature T and pressure p_0 , and a_{ij} and b_j are parameters which were adjusted to minimize the residual sum of squares. The coefficients are provided in Table 5. The values of the coefficients have been truncated to six decimal places for convenience, beyond which the results obtained

Table 3 Experimental values for the speed of sound of toluene c and standard uncertainty $u(c)$ as a function of pressure p and temperature T measured at UWA

T/K	p/MPa	$c/\text{m}\cdot\text{s}^{-1}$	$u(c)/\text{m}\cdot\text{s}^{-1}$
306.17	0.13	1269.90	0.19
306.19	0.53	1272.06	0.19
306.20	1.07	1274.93	0.18
306.16	2.41	1282.21	0.18
306.41	2.43	1279.22	0.18
306.42	4.99	1292.62	0.18
306.24	5.47	1297.90	0.18
306.43	10.58	1320.96	0.18
306.22	10.67	1324.17	0.18
306.43	14.35	1339.30	0.18
306.23	15.10	1345.59	0.18
306.34	16.72	1350.95	0.18
306.23	19.28	1365.11	0.18
306.42	20.29	1367.14	0.18
306.29	24.02	1384.63	0.18
306.31	24.32	1385.92	0.18
306.24	24.84	1390.16	0.18
306.32	25.21	1389.81	0.18
306.28	28.20	1403.11	0.18
306.21	29.77	1411.70	0.18
306.24	29.84	1411.89	0.18
306.10	30.14	1413.70	0.18
306.30	30.40	1412.49	0.18
306.17	32.46	1423.24	0.18
306.30	35.08	1432.10	0.18
306.30	35.11	1432.20	0.18
306.18	41.06	1458.18	0.18
306.18	45.10	1474.01	0.18
306.14	47.84	1484.75	0.18
306.11	51.38	1498.10	0.18
306.17	59.43	1527.36	0.18
306.18	59.78	1528.58	0.18
306.19	64.67	1545.85	0.18
320.45	0.17	1209.59	0.19
320.38	0.49	1211.71	0.19
320.38	1.21	1215.84	0.18
320.38	2.40	1222.63	0.18
320.46	4.04	1223.87	0.18
320.41	5.10	1237.70	0.18
320.46	5.51	1231.91	0.18
320.41	10.40	1266.19	0.18
320.31	10.60	1267.74	0.18
320.31	10.60	1267.74	0.18

Table 3 (continued)

T/K	p/MPa	$c/m\cdot s^{-1}$	$u(c)/m\cdot s^{-1}$
320.42	12.73	1269.97	0.18
320.39	19.58	1312.50	0.18
320.55	19.58	1303.15	0.18
320.45	25.92	1332.98	0.17
320.48	26.12	1333.78	0.17
320.45	30.11	1361.11	0.17
320.47	33.53	1376.21	0.17
320.46	39.80	1403.01	0.17
320.42	45.16	1425.21	0.17
320.42	45.16	1425.19	0.17
320.40	49.98	1444.44	0.17
320.40	49.98	1444.44	0.17
320.46	53.00	1456.00	0.17
320.46	53.01	1456.01	0.17
320.42	59.61	1481.06	0.17
320.42	59.61	1481.08	0.17
320.41	65.03	1500.95	0.18
320.41	65.04	1500.98	0.18
343.35	0.11	1114.66	0.19
343.36	0.11	1114.63	0.19
343.37	0.56	1117.55	0.19
343.38	0.57	1117.63	0.19
343.38	1.04	1120.63	0.19
343.38	1.04	1120.69	0.19
343.39	2.72	1131.30	0.19
343.39	2.72	1131.35	0.19
343.42	5.27	1147.11	0.18
343.42	5.27	1147.15	0.18
343.43	10.41	1177.63	0.18
343.43	10.41	1177.65	0.18
343.26	10.94	1181.38	0.18
343.27	10.95	1181.41	0.18
343.44	15.07	1203.83	0.18
343.37	19.36	1227.23	0.18
343.40	25.37	1258.02	0.17
343.41	31.31	1287.05	0.17
343.42	34.92	1303.94	0.17
343.39	44.67	1347.66	0.17
343.40	50.99	1374.36	0.17
343.38	55.43	1392.66	0.17
343.37	58.02	1403.03	0.17
343.37	58.02	1403.06	0.17
343.40	65.05	1430.40	0.17

Table 3 (continued)

T/K	p/MPa	$c/\text{m}\cdot\text{s}^{-1}$	$u(c)/\text{m}\cdot\text{s}^{-1}$
343.40	65.06	1430.42	0.17
363.18	0.11	1035.00	0.21
363.17	4.86	1068.34	0.20
363.20	9.90	1101.15	0.19
363.20	9.90	1101.21	0.19
363.14	10.88	1107.61	0.19
363.20	19.76	1160.19	0.18
363.20	19.76	1160.17	0.18
363.22	25.13	1189.66	0.18
363.22	30.04	1215.40	0.17
363.21	35.18	1241.19	0.17
363.17	40.05	1264.84	0.17
363.19	44.94	1287.48	0.17
363.19	50.07	1310.39	0.17
363.19	55.18	1332.43	0.17
363.17	60.79	1355.89	0.17
363.15	64.55	1371.16	0.17
363.16	64.58	1371.24	0.17
383.44	0.11	955.06	0.22
383.44	0.55	958.63	0.22
383.45	1.06	962.79	0.22
383.43	9.94	1028.75	0.21
383.44	19.70	1092.02	0.19
383.44	19.71	1092.01	0.19
383.43	24.87	1122.69	0.19
383.39	29.79	1150.45	0.19
383.39	29.79	1150.45	0.19
383.42	35.01	1178.26	0.18
383.42	35.01	1178.27	0.18
383.43	40.28	1205.08	0.18
383.40	44.78	1227.21	0.18
383.40	50.11	1252.28	0.18
383.41	54.92	1274.13	0.18
383.39	59.86	1295.90	0.17
383.35	64.88	1317.23	0.18
383.35	64.88	1317.23	0.18
403.10	0.29	880.19	0.26
403.11	0.55	882.54	0.26
403.07	1.16	888.19	0.26
403.08	2.89	903.45	0.25
403.11	10.08	961.23	0.24
403.06	16.11	1004.91	0.22
403.10	20.06	1031.25	0.22

Table 3 (continued)

T/K	p/MPa	$c/\text{m}\cdot\text{s}^{-1}$	$u(c)/\text{m}\cdot\text{s}^{-1}$
403.10	20.06	1031.30	0.22
403.04	29.68	1090.66	0.20
403.05	29.69	1090.72	0.20
403.05	34.85	1120.01	0.20
403.05	34.85	1119.99	0.20
403.05	39.99	1147.76	0.19
403.05	39.99	1147.75	0.19
403.06	44.29	1169.94	0.19
403.06	44.29	1169.99	0.19
403.08	50.60	1201.06	0.19
403.06	54.84	1221.20	0.19
403.04	59.96	1244.64	0.19
403.04	64.55	1265.03	0.19
422.63	0.30	804.97	0.32
422.63	0.30	804.99	0.32
422.65	0.73	809.37	0.32
422.65	0.73	809.39	0.32
422.62	1.04	812.59	0.31
422.63	1.04	812.62	0.31
422.63	2.69	828.98	0.31
422.63	2.69	829.04	0.30
422.66	5.08	851.58	0.30
422.57	8.28	880.24	0.28
422.58	8.28	880.28	0.28
422.55	11.28	905.36	0.27
422.54	11.28	905.37	0.26
422.60	14.92	933.70	0.25
422.61	14.93	933.79	0.26
422.63	20.87	976.80	0.24
422.63	20.87	976.83	0.25
422.62	24.86	1003.67	0.24
422.62	24.86	1003.66	0.24
422.65	31.56	1045.82	0.23
422.65	31.56	1045.85	0.23
422.63	34.90	1065.74	0.22
422.63	34.90	1065.72	0.22
422.60	39.92	1094.35	0.22
422.60	39.93	1094.36	0.22
422.59	44.96	1121.61	0.21
422.60	44.97	1121.68	0.21
422.58	50.05	1148.00	0.21
422.58	50.05	1147.99	0.21
422.58	54.88	1171.98	0.21

Table 3 (continued)

T/K	p/MPa	$c/\text{m}\cdot\text{s}^{-1}$	$u(c)/\text{m}\cdot\text{s}^{-1}$
422.58	54.88	1171.99	0.21
422.59	59.89	1195.82	0.20
422.59	59.90	1195.85	0.21
422.75	64.29	1215.66	0.21

Standard uncertainty of temperature $u(T)$: 0.03 K for $T=(306, 320, \text{ and } 343)$ K; 0.04 K for $T=(363 \text{ and } 383)$ K; 0.05 K for $T=403$ K; 0.07 K for $T=423$ K. Standard uncertainty of pressure, $u(p)=0.02$ MPa

from the fit were found to vary insignificantly. For instance, the maximum deviation between the truncated coefficients and actual coefficients upon which the results presented in this study are based was less than 0.5 parts per million. The goodness of fit of the speed-of-sound surface correlation was quantified by analysing the Average Absolute Relative Deviations (Δ_{AARD}) and Maximum Absolute Relative Deviation (Δ_{MARD}).

The experimental speeds of sound from UWA and ICL are compared with the correlation in Figs. 2 and 3, while the relative deviations are shown in Fig. 4. The goodness-of-fit metrics are $\Delta_{\text{AARD}}=0.01\%$, $\Delta_{\text{MARD}}=0.08\%$ (found at $T=373.15$ K and $p=60$ MPa) and the 95% confidence interval of the average relative deviations is between (0.012 and 0.016)%. Approximately 85% of the experimental dataset is fitted with absolute relative deviations of $\leq 0.02\%$, while 96% of the data set is fitted with absolute relative deviations of $\leq 0.03\%$. The effect of outlying data on the surface correlation was assessed and confirmed to not significantly influence the fit.

5 Comparison of Speed of Sound with Literature Data

In this section, our sound-speed data are compared against the Helmholtz EOS of Lemmon and Span [4] as well as the most accurate experimental data currently available for toluene in the investigated region. The relative deviations of the EOS and literature experimental data from the surface fit correlated to our data (which is chosen as the baseline) are plotted against pressures at various experimental isotherms used in this study as shown in Figs. 5 and 6.

At pressures up to 100 MPa and at all temperatures, the Helmholtz EOS of Lemmon and Span [4] represents our data to within its reported uncertainty of 1% in that range. At higher pressures, the values obtained from EOS vary from our correlation by up to 2.1% which is close to the reported EOS uncertainty of 2%. The deviations are the greatest at the highest pressures of the isotherms $T=(373.15 \text{ and } 383.41)$ K. The maximum and average deviations of the EOS from our correlation are summarized in Table S1 of the supplementary information section.

Comparisons were also made against other models but have not been presented graphically owing to their very high deviations from the available literature and our experimental data. In summary, the EOS of Polt et al. [22] within the range of its

Table 4 Experimental values for the speed of sound of toluene c and standard uncertainty $u(c)$ as a function of pressure p and temperature T measured at ICL

T/K	p/MPa	$c/m\cdot s^{-1}$	$u(c)/m\cdot s^{-1}$
283.15	30.19	1502.39	0.90
283.15	60.14	1609.63	0.97
283.15	90.04	1703.20	1.02
283.15	120.24	1787.54	1.07
283.15	149.99	1863.04	1.12
283.15	180.43	1934.00	1.16
283.15	210.03	1997.94	1.20
283.15	240.31	2059.12	1.24
283.15	269.98	2115.45	1.27
283.15	300.05	2169.82	1.30
283.15	330.05	2221.18	1.33
283.15	360.25	2270.54	1.36
283.15	389.98	2317.01	1.39
298.15	30.08	1443.49	0.87
298.15	60.20	1557.01	0.93
298.15	90.13	1654.39	0.99
298.15	119.97	1740.39	1.04
298.15	150.23	1819.34	1.09
298.15	180.19	1891.02	1.13
298.15	210.16	1957.36	1.17
298.15	240.26	2019.46	1.21
298.15	270.46	2078.03	1.25
298.15	300.15	2132.53	1.28
298.15	329.91	2184.37	1.31
298.15	360.02	2234.29	1.34
298.15	390.01	2282.09	1.37
323.15	30.00	1350.79	0.81
323.15	60.17	1473.56	0.88
323.15	90.20	1577.76	0.95
323.15	120.66	1670.01	1.00
323.15	150.27	1750.52	1.05
323.15	179.98	1824.20	1.09
323.15	210.22	1893.85	1.14
323.15	240.02	1957.41	1.17
323.15	270.09	2017.64	1.21
323.15	300.07	2074.27	1.24
323.15	330.00	2127.69	1.28
323.15	360.29	2179.26	1.31
323.15	389.93	2227.48	1.34
348.15	30.15	1265.36	0.76
348.15	60.13	1395.96	0.84
348.15	90.31	1506.73	0.90
348.15	120.32	1602.26	0.96

Table 4 (continued)

T/K	p/MPa	$c/m\cdot s^{-1}$	$u(c)/m\cdot s^{-1}$
348.15	150.46	1687.69	1.01
348.15	180.23	1764.23	1.06
348.15	210.54	1836.00	1.10
348.15	240.10	1900.99	1.14
348.15	270.60	1963.70	1.18
348.15	300.32	2021.20	1.21
348.15	330.13	2075.74	1.25
348.15	360.14	2127.73	1.28
348.15	390.00	2176.92	1.31
373.15	30.07	1183.47	0.71
373.15	60.00	1323.42	0.79
373.15	90.34	1440.60	0.86
373.15	120.24	1540.23	0.92
373.15	150.34	1628.84	0.98
373.15	180.20	1708.20	1.02
373.15	210.11	1781.11	1.07
373.15	240.27	1849.24	1.11
373.15	270.18	1912.25	1.15
373.15	300.19	1971.49	1.18
373.15	330.35	2027.37	1.22
373.15	360.55	2080.74	1.25
373.15	390.03	2130.48	1.28
398.15	30.07	1107.29	0.66
398.15	60.01	1256.71	0.75
398.15	90.31	1379.44	0.83
398.15	120.39	1483.63	0.89
398.15	150.32	1574.92	0.94
398.15	180.22	1656.81	0.99
398.15	210.00	1731.10	1.04
398.15	240.20	1800.46	1.08
398.15	270.09	1864.90	1.12
398.15	300.00	1925.01	1.16
398.15	330.09	1982.29	1.19
398.15	360.01	2036.20	1.22
398.15	390.00	2088.55	1.25
423.15	30.08	1035.61	0.62
423.15	60.12	1194.96	0.72
423.15	90.12	1322.02	0.79
423.15	120.03	1429.30	0.86
423.15	150.23	1524.26	0.91
423.15	180.33	1608.84	0.97
423.15	210.09	1684.92	1.01
423.15	240.21	1755.96	1.05

Table 4 (continued)

<i>T</i> /K	<i>p</i> /MPa	<i>c</i> /m·s ⁻¹	<i>u</i> (<i>c</i>)/m·s ⁻¹
423.15	270.10	1821.45	1.09
423.15	300.10	1883.03	1.13
423.15	329.96	1940.82	1.16
423.15	360.00	1997.13	1.20
423.15	390.00	2049.64	1.23
448.15	30.30	969.48	0.58
448.15	59.95	1136.31	0.68
448.15	90.25	1269.95	0.76
448.15	119.95	1379.82	0.83
448.15	150.22	1477.59	0.89
448.15	180.07	1563.71	0.94
448.15	209.85	1641.64	0.98
448.15	240.09	1714.35	1.03
448.15	270.23	1781.81	1.07
448.15	300.00	1844.24	1.11
448.15	330.05	1904.07	1.14
448.15	360.26	1960.61	1.18
448.15	389.97	2013.46	1.21
473.15	30.06	903.93	0.54
473.15	60.11	1082.96	0.65
473.15	90.33	1221.13	0.73
473.15	120.36	1335.44	0.80
473.15	150.13	1434.05	0.86
473.15	180.09	1522.51	0.91
473.15	210.21	1603.20	0.96
473.15	240.00	1676.68	1.01
473.15	269.85	1745.42	1.05
473.15	300.11	1810.67	1.09
473.15	330.02	1869.02	1.12
473.15	360.02	1926.03	1.16
473.15	390.03	1979.82	1.19

Standard uncertainties are *u*(*T*)=0.015 K and *u*(*p*)=Max(0.025 MPa, 0.0006·*p*).

Table 5 Coefficients of fit of correlations of Eqs. 1 and 2

<i>a</i> ₁₀	-1.148868×10^{-1}	<i>a</i> ₁₁	1.061382×10^{-1}	<i>a</i> ₁₂	4.474984×10^{-1}	<i>a</i> ₁₃	-2.496091×10^{-1}
<i>a</i> ₂₀	-4.373371×10^{-4}	<i>a</i> ₂₁	1.736190×10^{-3}	<i>a</i> ₂₂	-1.812275×10^{-3}	<i>a</i> ₂₃	6.885332×10^{-4}
<i>a</i> ₃₀	1.208315×10^{-7}	<i>a</i> ₃₁	-3.691194×10^{-7}	<i>a</i> ₃₂	5.146784×10^{-7}	<i>a</i> ₃₃	-2.289112×10^{-7}
<i>b</i> ₀	2.958112×10^3	<i>b</i> ₁	-2.146336×10^3	<i>b</i> ₂	5.986051×10^3	<i>b</i> ₃	-1.140723×10^2

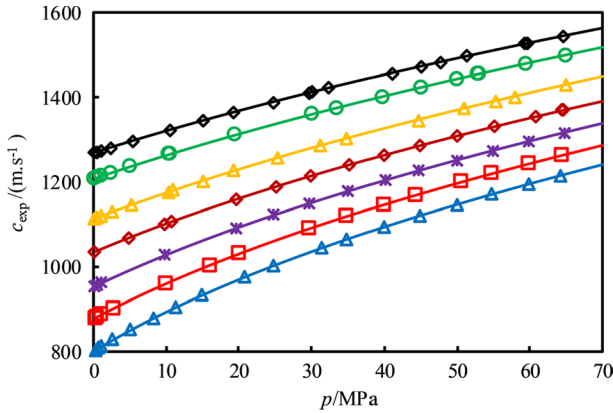


Fig. 2 Experimental speed of sound, c_{exp} , in liquid toluene as a function of pressure measured at UWA. \diamond , $T=306.19$ K; \circ , $T=320.41$ K; \triangle , $T=343.38$ K; \diamond , $T=363.19$ K; $*$, $T=383.41$ K; \square , $T=403.07$ K; \triangle , $T=422.62$ K. Lines represent the values evaluated from the correlation of Eqs. 1 and 2

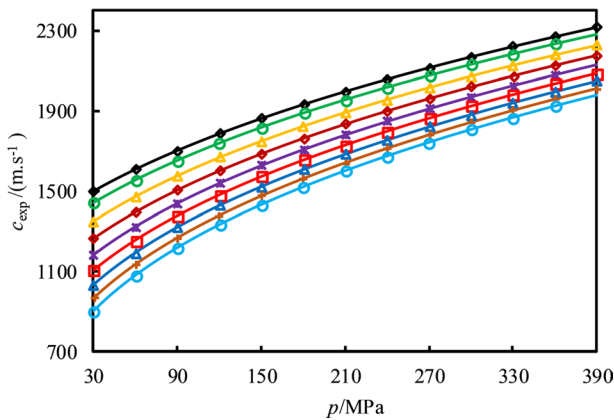


Fig. 3 Experimental speed of sound, c_{exp} , in liquid toluene as a function of pressure measured at ICL. \diamond , $T=283.15$ K; \circ , $T=298.15$ K; \triangle , $T=323.15$ K; \diamond , $T=348.15$ K; $*$, $T=373.15$ K; \square , $T=398.15$ K; \triangle , $T=423.15$ K; $+$, $T=448.15$ K; \circ , $T=473.15$ K. Lines represent the values evaluated from the correlation of Eqs. 1 and 2

validity of up to 25 MPa in pressure deviates from our data by up to nearly 2% at the highest pressures along all isotherms. At higher pressures, for all temperatures, their EOS overpredicts sound speed relative to our data with the deviations increasing with increasing pressure. The non-analytical EOS of Goodwin [23] at selected pressures follows a similar trend, consistently overpredicting sound speed relative to our data at the lowest pressures with deviations of up to 5% at the lowest isotherm and lowest pressures. At other points of pressure and temperature, the deviations fall within 2%.

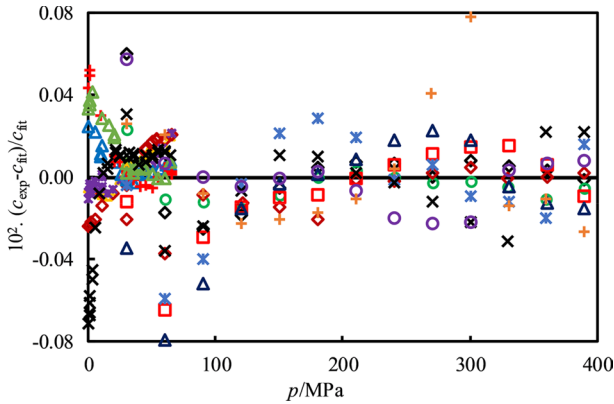


Fig. 4 Relative percentage deviations of the combined experimental speed-of-sound data measured at UWA and ICL, c_{exp} , from the combined surface fit, c_{fit} , values calculated by using Eqs. 1 and 2. \diamond , $T=283.15$ K; \circ , $T=298.15$ K; \triangle , $T=323.15$ K; \diamond , $T=321.42$ K; $*$, $T=343.38$ K; \square , $T=348.15$ K; \triangle , $T=363.19$ K; \triangle , $T=373.15$ K; $+$, $T=383.41$ K; $*$, $T=398.15$ K; \triangle , $T=403.04$ K; \times , $T=422.76$ K; \circ , $T=448.15$ K; $+$, $T=473.15$ K

Our correlated data most closely and consistently agree with the experimental data of Meier et al. [17]. Most of the deviations are within the reported uncertainty of their data of 0.03%. Deviations of up to 0.06% from their data occur at the lowest pressures at $T=300$ K; however, this is within the mutual uncertainties of both experiments. The data from Okhotin et al. [15] also show close agreement with our data with most of the deviations falling within the reported experimental uncertainty of 0.05% with average deviations below 0.03% for all isotherms. However, larger deviations of up to 0.12% are observed at $p=0.1$ MPa at $T=383.12$ K, which is close to the normal boiling point of $T=383.75$ K. The data from Vervieko et al. [16] at $T=(293, 323$ and $373)$ K are consistently lower than our data at all pressures, except at $p=0.1$ MPa. The highest deviations of up to 0.7% occur at their highest reported pressure of $p=250$ MPa. Similarly, the data from Muringer et al. [14] at $T=(298.14$ and $320.29)$ K are consistently close to 0.2% higher than our data with the highest deviation of 0.3% occurring at the atmospheric pressure, $p=0.1$ MPa. The 2017 data by Yebra et al. [18] at $T=(303.15, 323.15$ and $343.15)$ K have average deviations of close to 0.1% from our data. However, at the highest pressure of $p=60.1$ MPa and at atmospheric pressures, deviations of up to 0.2% are observed.

6 Derived Thermodynamic Properties and Uncertainties

Thermodynamic properties over the investigated ranges of temperature and pressure can be derived with very high accuracy from the sound-speed surface by means of numerical integration of the following partial differential equations (PDEs) [24]:

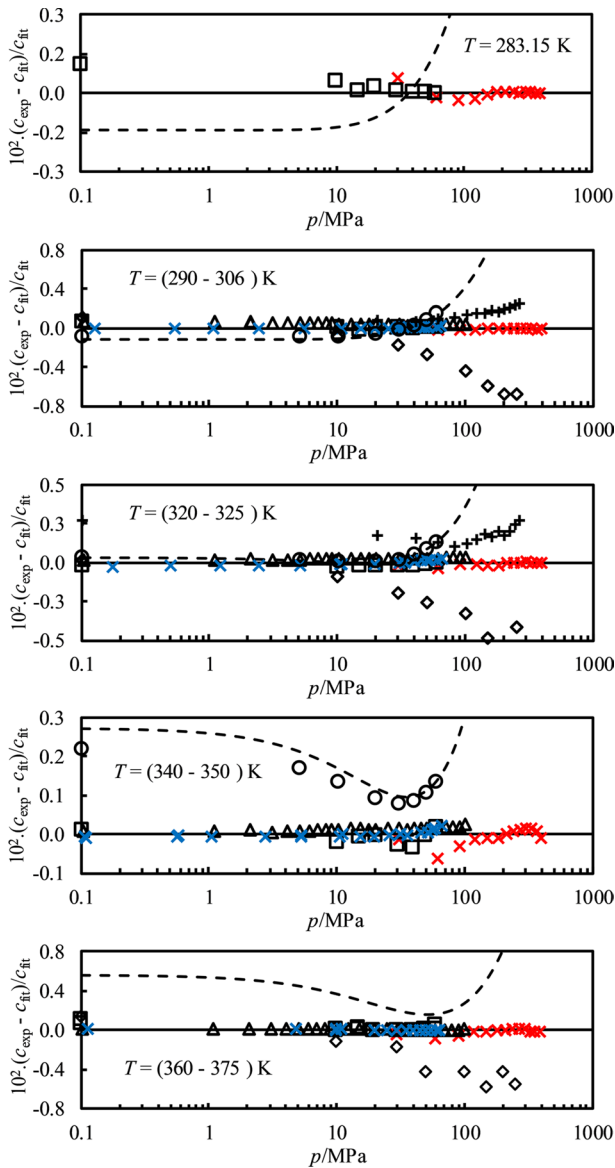


Fig. 5 Relative percentage deviations for experimental literature data (c_{exp} , symbols) and the Helmholtz EOS [4] (dotted lines), calculated relative to the surface-fit correlation of this work (baseline), c_{fit} . Deviations are presented as a function of pressure at temperatures in the vicinity of the experimental isotherms used in this work. Experimental data: \times , UWA; \times , ICL; Δ , Meier et al. [17] at 300 K, 320 K, 340 K and 360 K; \circ , Yebra et al. [18] at 303.15 K, 323.15 K and 343.15 K; \diamond , Vervieko et al. [16] at 323 K and 373 K; $+$, Muringer et al. [14] at 298.14 K and 320.29 K and \square , Okhotin et al. [15] at 283.19 K, 293.15 K, 323.14 K, 343.14 K, 363.12 K and 373.12 K. EOS: —, Lemmon and Span [4]

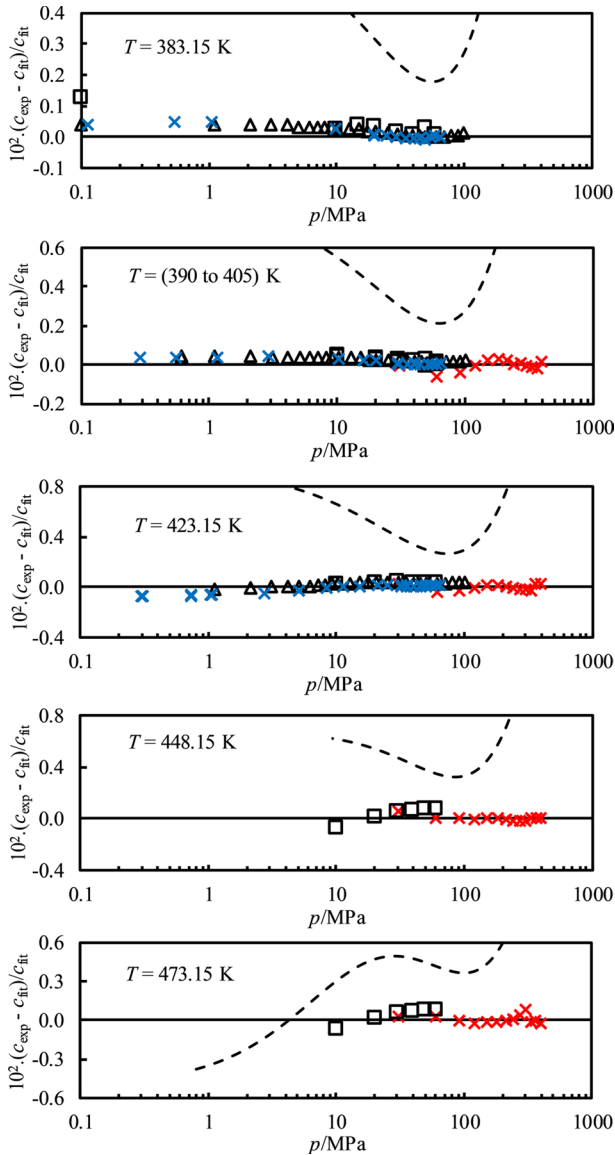


Fig. 6 Relative percentage deviations for experimental literature data (c_{exp} , symbols) and the Helmholtz EOS [4] (dotted lines), calculated relative to the surface-fit correlation of this work (baseline), c_{fit} . Deviations are presented as a function of pressure at temperatures in the vicinity of the experimental isotherms used in this work. Experimental data: \times , UWA; \times , ICL; Δ , Meier et al. [17] at 380 K, 400 K and 420 K and \square , Okhotin et al. [15] at 383.12 K, 393.12 K, 403.12 K, 423.11 K, 443.11 K, and 473.11 K, EOS: —, Lemmon and Span [4]

$$\begin{aligned}
 c^{-2} &= \left(\frac{\partial \rho}{\partial p}\right)_T - \left(\frac{T}{\rho^2 C_p}\right) \left(\frac{\partial \rho}{\partial T}\right)_p, \\
 \left(\frac{\partial C_p}{\partial p}\right)_T &= -\left(\frac{T}{\rho^3}\right) \left[2\left(\frac{\partial \rho}{\partial T}\right)_p^2 - \rho \left(\frac{\partial^2 \rho}{\partial T^2}\right)_p\right].
 \end{aligned}
 \tag{3}$$

The solutions of these PDEs are subject to prescribed initial values of density and specific heat capacity along the isobar at $p=p_0=0.1$ MPa. For the initial densities, a correlation was created by first extrapolating the low-uncertainty experimental data of McLinden and Splett [25] and Tay and Trusler [21] to p_0 and then correlating the results in terms of the equation:

$$\frac{\rho_{0,T}}{\text{kg}\cdot\text{m}^{-3}} = \sum_{j=1}^3 d_j \left(\frac{3T}{T_0}\right)^{e_j},
 \tag{4}$$

with coefficients d_j and exponents e_j as adjustable parameters. The data were weighted based on the experimental uncertainties, and an optimum solution was obtained by minimizing the weighted residual sum of squares. Similarly, a third-order polynomial fit was used to correlate the isobaric heat capacity based on the experimental data of Akhundov et al. [26], Chirico and Steele [27], Cerdeiriña et al. [28], and Perderson et al. [29] and in terms of the equation:

$$C_{p0,T}/\text{J}\cdot\text{kg}^{-1}\cdot\text{K}^{-1} = 1000 \times \sum_{j=0}^3 g_j \left(\frac{T}{T_0}\right)^j,
 \tag{5}$$

with coefficients g_j as an adjustable parameter. The values at high pressures were extrapolated to $p=p_0$, while those pertaining to saturation condition were corrected to the (possibly hypothetical) state at $p=p_0$ with the help of the EOS of Lemmon and Span [4]. The coefficients of the correlations of Eqs. 4 and 5 are provided in Table 6.

The PDEs, Eq. 3, were integrated using a predictor–corrector algorithm implemented in MATLAB R2019b. Prediction of the density, ρ , and isobaric heat capacity, C_p , at each temperature and pressure grid point was carried out by first-order Taylor series expansion, and the predicted values were corrected by using a more accurate mid-point formula as employed by Davila and Trusler [30]. Temperature derivatives of ρ and C_p at each grid point were obtained by means of third-order

Table 6 Coefficients of fit of correlations of Eqs. 4^a and 5^b for various reference pressures

j	d_j	e_j	g_j
0	–	–	1.054785
1	1.123743×10^3	0.000	0.517658
2	-8.354357×10^1	1.042	0.036530
3	-1.600587×10^{-4}	7.765	0.105107

Weighted sum of squares of errors: ^aWSSQ=0.043. ^bWSSQ=0.0045.

polynomial fitting, which was found to sufficiently represent the calculated data. Rigorous mesh-dependency tests were carried out to ensure that the algorithm implemented was insensitive to the grid of spacings defined by $(\Delta T, \Delta p)$. Trial step sizes for temperature were $\Delta T = (10, 5, 2.5 \text{ and } 1) \text{ K}$. The differences in the derived densities for all trial grids were less than 9 ppm overall with convergence as the grid size were lowered. The difference between 2.5 K and 1 K grid sizes for density results was less than 3 ppm along all isobars and isotherms. The results in isobaric heat capacity showed similar behaviour with the maximum difference in values between temperature grids of 2.5 K and 1 K being less than 70 ppm. Therefore, $\Delta T = 1 \text{ K}$ was chosen as the final temperature grid size as the computational time did not increase significantly. Similarly, step sizes for pressure were varied between $\Delta p = (0.1 \text{ and } 0.01) \text{ MPa}$ with resulting variation in density of less than 0.07 ppm and isobaric heat capacity of less than 0.25 ppm throughout the whole range of integration. Finally, the pressure grid size of $\Delta p = 0.1 \text{ MPa}$ was chosen for computational efficiency. Since these variations are much less than the typical uncertainties of the most accurate available data for density and isobaric heat capacity of toluene, i.e. 500 ppm and 5000 ppm, respectively, it can be concluded that the chosen step sizes of pressure and temperature render the numerical error in the integration algorithm negligible. These results suggest that the implemented algorithm is mesh independent within the allowable limits of uncertainties.

The accuracy of the derived thermodynamic properties is dependent upon the speed-of-sound surface employed as well as the initial values of density and heat capacities imposed along the isobar at $p = p_0$. However, the evaluation of uncertainties of the derived properties obtained from the thermodynamic integration of sound-speed data is a non-trivial problem. The typical way of estimating these uncertainties is to study empirically the effect on the derived properties of variation of input parameters by a fixed percentage. Trusler and Lemmon [31] advocated a more comprehensive strategy in which these parameters are subject to both constant and oscillatory perturbations. In the remainder of this section, a brief description of the methodology is provided, and its application in this work is explained. Here, we follow the same methodology detailed in [31] with the only difference being in the way in which the temperature derivatives are calculated.

Defining an arbitrary dimensionless number $\varepsilon \ll 1$ and a function f_1 of the order of unity, the perturbed speed of sound c' related to the true speed of sound by

$$\frac{1}{c'^2} = \frac{1 + \varepsilon f_1}{c^2}. \quad (6)$$

Similarly, the perturbed values of ρ and C_p can be stated as follows:

$$\rho' = \rho(1 + \varepsilon f_2), \text{ and} \quad (7)$$

$$C_p' = C_p(1 + \varepsilon f_3) \quad (8)$$

Substitution of the perturbed quantities in Eq. 3 and isolation of the first-order terms in ε lead to the following auxiliary PDEs:

$$\begin{aligned} \rho \left(\frac{\partial f_2}{\partial p} \right)_T &= \left(\frac{f_1 - f_2}{c^2} \right) - \left(\frac{T \alpha_p^2}{C_p} \right) \left[f_2 + f_3 + \frac{2}{\alpha_p} \left(\frac{\partial f_2}{\partial T} \right)_p \right], \\ \left(\frac{\partial (C_p f_3)}{\partial p} \right)_T &= T \left(\frac{\partial^2 (f_2 / \rho)}{\partial T^2} \right)_p, \end{aligned} \tag{9}$$

where

$$\alpha_p = -\rho^{-1} \left(\frac{\partial \rho}{\partial T} \right)_p. \tag{10}$$

These auxiliary PDEs relate the functions f_1, f_2 , and f_3 . For example, if the sound speed is perturbed according to Eq. 6 with a prescribed function $f_1(T, p)$, then the resulting perturbation functions f_2 and f_3 can be obtained from Eq. 9.

Here, we define the oscillatory function of temperature and/or pressure with wavenumbers for the i th term of

$$k_i = \frac{2\pi}{\lambda_i}, \tag{11}$$

where λ_i is a wavelength in temperature or pressure units. The imposed perturbations to the sound-speed surface, f_1 , initial density, $f_{2,0}$, and initial isobaric heat capacity, $f_{3,0}$ are then defined as follows:

$$f_1(T, p) = A_1 \cos(k_1 T) \cos(k_4 p), \tag{12}$$

$$f_{2,0}(T) = A_2 \cos(k_2 T), \text{ and} \tag{13}$$

$$f_{3,0}(T) = A_3 \cos(k_3 T), \tag{14}$$

where the amplitudes are given by $A_i = 1$ or 0 , according to where the corresponding perturbations are switched on or off. Calculations were carried out for both constant ($k_j = 0$) and dynamic/variable ($k_j > 0$) perturbations.

The PDEs of Eq. 9 were also implemented in MATLAB and solution was achieved with initial assumed perturbations of $f_1, f_{2,0}$, and $f_{3,0}$ by employing Euler’s first-order expansion method as described by Trusler and Lemmon [31].

The main difficulty in this method arises during the evaluation of the derivatives of temperature in Eq. 9. Since the dynamic perturbations ($k_j > 0$) we have in this study are sinusoidal in nature, we employed a six-variable second-order sum-of-sine fit to relate the quantities f_2 and f_2/ρ as functions of temperature along individual isobars. The equation of fit employed is given by

$$X = \sum_{j=1}^2 A_j \sin(B_j T + C_j), \tag{15}$$

where X is either f_2 or f_2/ρ . These fitted quantities were then differentiated with respect to temperature along each isobar.

The choice of order of fit for the dynamic perturbations was made after an extensive analysis of fit at various isobars. The fit coefficients vary at each isobar with the variation in the values of f_2 and ρ . The improvement in sum-of-sine fit from first order to second order was found to be significant with the sum of squares errors more than eight orders of magnitude lower than this increase in order of fit. Hence, the second-order sum-of-sine fit was employed to fit the temperature derivatives of Eq. 9. This higher-order fit also ensures that the more rapid fluctuations owing to high k_j values are well explained. In the case of constant perturbations ($k_j=0$), a second-order polynomial fit was found to sufficiently represent the fitted data.

To illustrate the overall nature of dynamic perturbations on the derived properties, k_1 , k_2 and k_3 were selected from values of (0.025, 0.05, 0.1 and 0.2) K^{-1} , corresponding to wavelengths of about (251, 125, 63 and 31) K, while k_4 was zero, 0.03 MPa^{-1} or 0.05 MPa^{-1} . The results of the sensitivity analysis are summarized in Table 7 which includes various scenarios of constant and dynamic perturbations. A selection of the results is also represented graphically in Figures S1 to S6 of the Supplementary Information.

These results illustrate the negative impact of temperature-dependent fluctuations in any of the input quantities on the derived isobaric heat capacity and isobaric expansivity. When the cyclic variations of sound speed with pressure are also considered, the perturbations decrease significantly. These observations suggest that the cyclic variation with pressure reduces the negative impact of variations with respect to temperature. Since the effect of f_1 at a given temperature oscillates with increasing pressure and is not constant, the reduction in the effect of sound-speed perturbation on derived property perturbation functions is reasonable. These observations are consistent with those made by Trusler and Lemmon [31].

Constant perturbations of the input parameters have a minimal effect on the derived properties. However, dynamic perturbations in input quantities lead to higher perturbations in derived properties. Particularly, the short wavelength perturbations have the most negative impact on the derived properties with the resulting perturbations being orders of magnitude higher than in the case of slowly varying perturbations in temperature. These observations suggest that fit of sound-speed data needs to be such that these perturbations do not vary rapidly with increasing temperature. The fit deviations in this study do not vary rapidly with temperature.

Following these observations, the uncertainties in derived properties in this study were estimated by considering the average of constant perturbations and dynamic perturbations (cf. Table 7, Cases I to V) resulting from the input perturbations equivalent to the experimental uncertainty of the experimental sound-speed data (0.08%) and the highest uncertainties in initial values of density (0.1%) and isobaric heat capacity (1%) from the experimental data that were used for correlations. For an arbitrary derived property, z , the overall standard uncertainty was estimated by

Table 7 Summary of results of sensitivity analysis depicting average and maximum deviations of perturbed quantities from derived quantities as results of constant and dynamic perturbations

Case	Pert type	Pert quantity	Switches			Repeccency				Pert. amount, ϵ (%)	Δ_{MARD} (%)					
			A_1	A_2	A_3	k_1 (K ⁻¹)	k_2 (K ⁻¹)	k_3 (K ⁻¹)	k_4 (MPa ⁻¹)		ρ	C_p	α_p	ρ	C_p	α_p
I	Constant	c	1	0	0	0	0	0	0	0.08	0.01	0.01	0.04	0.01	0.02	0.12
II	Constant	ρ_0	0	1	0	0	0	0	0	0.10	0.09	0.01	0.06	0.10	0.03	0.16
III	Constant	$C_{p,0}$	0	0	1	0	0	0	0	1.00	0.02	1.01	0.07	0.04	1.09	0.22
IV	Dynamic	c	1	0	0	0.025	0	0	0	0.08	0.01	0.08	0.15	0.01	0.39	0.58
V	Dynamic	c	1	0	0	0.025	0	0	0.03	0.08	0.00	0.03	0.06	0.00	0.15	0.23
VI	Dynamic	c	1	0	0	0.2	0	0	0	0.08	0.01	2.33	2.19	0.08	19.19	19.19
VII	Dynamic	c	1	0	0	0.1	0	0	0.05	0.08	0.00	0.41	0.38	0.02	2.81	1.94
VIII	Dynamic	c	1	0	0	0.2	0	0	0.05	0.08	0.01	2.21	2.25	0.06	20.13	16.19
IX	Dynamic	ρ_0	0	1	0	0	0.05	0	0	0.10	0.09	4.41	6.56	0.20	15.62	20.91
X	Dynamic	$C_{p,0}$	0	0	1	0	0	0.05	0	1.00	0.01	1.40	1.18	0.04	5.50	5.57

The deviations resulting from cases highlighted in bold were averaged and used in Eq. 16 to estimate expanded uncertainties of derived properties

$$u(z)^2 = \left(\frac{\partial z}{\partial c}\right)_{\rho_0, C_{p0}}^2 u(c)^2 + \left(\frac{\partial z}{\partial \rho_0}\right)_{c, C_{p0}}^2 u(\rho_0)^2 + \left(\frac{\partial z}{\partial C_{p0}}\right)_{c, \rho_0}^2 u(C_{p0})^2. \quad (16)$$

In the above equation, the first term on the right-hand side describes the influence of overall sound-speed measurement uncertainty on the derived property. Similarly, the second and third terms describe the influence of overall uncertainty of initial density and heat capacities. The uncertainties in density and isobaric heat capacity were estimated by means of constant input perturbations to Eq. 9 with the resulting perturbed values given by Eqs. 7 and 8. The uncertainties in the other derived properties described in this work were then evaluated by using the perturbed values of speed of sound, density, and isobaric heat capacities over the entire thermodynamic integration range. The overall expanded uncertainties of all derived properties are provided in Table 8.

Other thermodynamic properties were also calculated based on the correlated speed of sound and derived density and isobaric heat capacity values. Isothermal compressibility, κ_T , is determined according to the following relationship:

$$\kappa_T = \rho^{-1} \left(\frac{\partial \rho}{\partial p} \right)_T. \quad (17)$$

Isobaric expansivity, α_p was evaluated using the relation given by Eq. 10. Similarly, a useful relation for the speed of sound propagation which relates the density, heat capacities and isothermal compressibility with isentropic compressibility in fluid phases, κ_s , can be used to derive other thermodynamic properties [32]:

$$c^2 = \left(\frac{\partial p}{\partial \rho} \right)_s = \frac{1}{\rho \kappa_s} = \frac{C_p}{C_v \rho \kappa_T}. \quad (18)$$

The thermal pressure coefficient can be obtained as follows:

$$p_c = \left(\frac{\partial p}{\partial T} \right)_\rho = \frac{\alpha_p}{\kappa_T}. \quad (19)$$

Finally, the thermodynamic equation of state can be used to evaluate the internal pressure, p_{int} according to the relation:

$$p_{int} \equiv \left(\frac{\partial U}{\partial V} \right)_T = T \left(\frac{\partial p}{\partial T} \right)_\rho - p = T \frac{\alpha_p}{\kappa_T} - p. \quad (20)$$

All derived thermodynamic properties with the overall relative uncertainties over a range of selected isobars and isotherms are provided in Table 8.

Table 8 Derived thermodynamic properties of liquid toluene at isotherms T and selected isobars of pressures p

p/MPa	$c/(\text{m}\cdot\text{s}^{-1})^a$	$\rho/(\text{kg}\cdot\text{m}^{-3})$	$C_p/\text{J}\cdot\text{kg}^{-1}\cdot\text{K}^{-1}$	$C_p/\text{J}\cdot\text{kg}^{-1}\cdot\text{K}^{-1}$	$\alpha_p\cdot 10^6/\text{K}^{-1}$	$\kappa_T\cdot 10^6/\text{MPa}^{-1}$	$\kappa_S\cdot 10^6/\text{MPa}^{-1}$	$p_c/\text{MPa}\cdot\text{K}^{-1}$	$P_{\text{inf}}/\text{MPa}$
$T = 283 \text{ K}$									
0.1	1370.33	876.24	1661.75	1226.14	1053.99	823.66	607.75	1.2796	362.04
10	1417.04	883.19	1656.34	1222.97	1016.30	763.70	563.88	1.3308	366.61
50	1575.68	907.00	1642.04	1244.72	863.70	583.83	444.08	1.4743	367.23
100	1732.91	930.83	1636.94	1265.29	752.17	462.83	357.75	1.6252	359.92
120	1787.71	939.16	1636.99	1272.88	719.54	428.48	333.17	1.6793	355.24
150	1863.61	950.68	1638.39	1283.71	678.65	386.55	302.87	1.7557	346.86
180	1933.38	961.27	1640.91	1293.94	644.94	352.93	278.30	1.8274	337.15
210	1998.16	971.09	1644.20	1303.67	616.53	325.29	257.92	1.8953	326.37
240	2058.78	980.26	1648.04	1312.95	592.16	302.11	240.68	1.9601	314.71
270	2115.88	988.88	1652.28	1321.85	570.95	282.34	225.88	2.0222	302.29
300	2169.94	997.03	1656.81	1330.42	552.29	265.26	213.01	2.0820	289.22
330	2221.35	1004.77	1661.55	1338.69	535.69	250.34	201.70	2.1399	275.58
360	2270.43	1012.14	1666.46	1346.70	520.81	237.17	191.67	2.1959	261.43
390	2317.42	1019.19	1671.49	1354.47	507.35	225.46	182.70	2.2503	246.83
$T = 298 \text{ K}$									
0.1	1304.93	862.33	1708.04	1268.38	1080.15	917.06	681.01	1.1778	350.89
10	1354.51	869.87	1700.89	1270.03	1027.32	839.16	626.59	1.2242	354.82
50	1521.23	895.38	1683.57	1289.89	863.19	629.92	482.62	1.3703	358.36
100	1684.58	920.49	1677.33	1310.63	744.94	489.93	382.82	1.5205	353.11
120	1741.19	929.19	1677.19	1318.31	710.90	451.62	354.98	1.5741	349.09
150	1819.36	941.18	1678.44	1329.26	668.57	405.31	320.99	1.6495	341.56
180	1891.00	952.15	1680.91	1339.63	633.92	368.53	293.71	1.7201	332.60
210	1957.35	962.29	1684.21	1349.49	604.88	338.52	271.24	1.7869	322.48
240	2019.32	971.74	1688.09	1358.93	580.09	313.50	252.37	1.8503	311.40
270	2077.59	980.60	1692.41	1367.98	558.60	292.29	236.26	1.9111	299.51

Table 8 (continued)

p/MPa	$c/(\text{m}\cdot\text{s}^{-1})^a$	$\rho/(\text{kg}\cdot\text{m}^{-3})$	$C_p/\text{J}\cdot\text{kg}^{-1}\cdot\text{K}^{-1}$	$C_p/\text{J}\cdot\text{kg}^{-1}\cdot\text{K}^{-1}$	$\alpha_p\cdot 10^6/\text{K}^{-1}$	$\kappa_T\cdot 10^6/\text{MPa}^{-1}$	$\kappa_S\cdot 10^6/\text{MPa}^{-1}$	$p_c/\text{MPa}\cdot\text{K}^{-1}$	$P_{\text{int}}/\text{MPa}$
300	2132.67	988.96	1697.03	1376.71	539.75	274.05	222.32	1.9695	286.92
330	2184.98	996.88	1701.89	1385.13	523.03	258.17	210.12	2.0259	273.72
360	2234.84	1004.42	1706.91	1393.30	508.07	244.21	199.34	2.0805	259.99
390	2282.54	1011.61	1712.06	1401.22	494.59	231.82	189.74	2.1334	245.77
$T=306\text{ K}$									
0.1	1270.58	854.86	1732.97	1291.30	1095.38	972.44	724.60	1.1264	344.59
10	1321.88	862.74	1724.76	1294.78	1034.99	883.62	663.34	1.1713	348.42
50	1493.17	889.23	1705.64	1313.86	863.42	654.80	504.39	1.3186	353.49
100	1659.80	915.05	1698.72	1334.67	741.38	504.88	396.68	1.4684	349.33
120	1717.35	923.95	1698.46	1342.38	706.56	464.32	366.97	1.5217	345.64
150	1796.69	936.19	1699.60	1353.39	663.44	415.54	330.90	1.5966	338.55
180	1869.28	947.37	1702.01	1363.82	628.28	377.00	302.09	1.6665	329.96
210	1936.42	957.68	1705.30	1373.75	598.90	345.68	278.47	1.7325	320.16
240	1999.07	967.27	1709.19	1383.26	573.88	319.66	258.70	1.7953	309.36
270	2057.92	976.26	1713.53	1392.39	552.24	297.65	241.87	1.8553	297.73
300	2113.51	984.73	1718.19	1401.18	533.28	278.77	227.34	1.9130	285.37
330	2166.26	992.75	1723.08	1409.68	516.50	262.37	214.65	1.9686	272.38
360	2216.52	1000.38	1728.15	1417.92	501.50	247.98	203.47	2.0223	258.83
390	2264.58	1007.65	1733.34	1425.92	488.00	235.24	193.52	2.0745	244.79
$T=321\text{ K}$									
0.1	1207.13	840.73	1780.38	1334.99	1126.89	1088.60	816.27	1.0352	332.19
10	1261.97	849.34	1769.90	1340.65	1052.86	976.01	739.30	1.0787	336.28
50	1442.28	877.78	1747.01	1358.64	864.81	704.22	547.67	1.2280	344.20
100	1615.06	904.97	1738.65	1379.51	735.25	533.92	423.63	1.3771	342.04

Table 8 (continued)

p/MPa	$c/(\text{m}\cdot\text{s}^{-1})^a$	$\rho/(\text{kg}\cdot\text{m}^{-3})$	$C_p/\text{J}\cdot\text{kg}^{-1}\cdot\text{K}^{-1}$	$C_p/\text{J}\cdot\text{kg}^{-1}\cdot\text{K}^{-1}$	$\alpha_p/10^6/\text{K}^{-1}$	$\kappa_T/10^6/\text{MPa}^{-1}$	$\kappa_S/10^6/\text{MPa}^{-1}$	$\rho_c/\text{MPa}\cdot\text{K}^{-1}$	$P_{\text{int}}/\text{MPa}$
120	1674.33	914.26	1738.12	1387.27	698.92	488.84	390.17	1.4297	338.95
150	1755.78	926.98	1739.01	1398.36	654.29	435.18	349.94	1.5035	332.62
180	1830.08	938.55	1741.29	1408.89	618.16	393.18	318.13	1.5722	324.67
210	1898.65	949.19	1744.50	1418.93	588.14	359.31	292.25	1.6369	315.43
240	1962.50	959.06	1748.37	1428.55	562.68	331.34	270.73	1.6982	305.12
270	2022.38	968.29	1752.71	1437.79	540.74	307.81	252.50	1.7567	293.92
300	2078.87	976.97	1757.39	1446.70	521.59	287.71	236.84	1.8129	281.95
330	2132.42	985.18	1762.32	1455.31	504.68	270.31	223.22	1.8670	269.31
360	2183.39	992.97	1767.43	1463.65	489.61	255.10	211.25	1.9193	256.09
390	2232.08	1000.39	1772.68	1471.75	476.06	241.66	200.64	1.9700	242.36
$T=343\text{ K}$									
0.1	1116.15	819.67	1852.06	1400.67	1181.87	1294.91	979.31	0.9127	312.96
10	1176.94	829.55	1837.48	1407.00	1087.78	1136.53	870.27	0.9571	318.29
50	1371.42	861.17	1808.01	1424.10	869.21	783.84	617.40	1.1089	330.36
100	1553.17	890.50	1797.13	1444.90	727.63	578.99	465.51	1.2567	331.06
120	1614.87	900.38	1796.10	1452.68	688.98	526.57	425.89	1.3084	328.79
150	1699.28	913.84	1796.49	1463.83	642.03	465.09	378.97	1.3804	323.49
180	1775.95	925.99	1798.44	1474.43	604.42	417.64	342.40	1.4472	316.40
210	1846.48	937.12	1801.44	1484.55	573.43	379.79	312.98	1.5099	307.88
240	1911.98	947.40	1805.17	1494.25	547.32	348.82	288.74	1.5691	298.20
270	1973.29	956.98	1809.41	1503.57	524.94	322.94	268.36	1.6255	287.54
300	2031.02	965.97	1814.03	1512.57	505.49	300.98	250.96	1.6795	276.07
330	2085.66	974.45	1818.92	1521.27	488.39	282.07	235.91	1.7314	263.88
360	2137.61	982.48	1824.01	1529.69	473.20	265.61	222.75	1.7816	251.07

Table 8 (continued)

p/MPa	$c/(\text{m}\cdot\text{s}^{-1})^a$	$\rho/(\text{kg}\cdot\text{m}^{-3})$	$C_p/\text{J}\cdot\text{kg}^{-1}\cdot\text{K}^{-1}$	$C_p/\text{J}\cdot\text{kg}^{-1}\cdot\text{K}^{-1}$	$\alpha_p\cdot 10^6/\text{K}^{-1}$	$\kappa_T\cdot 10^6/\text{MPa}^{-1}$	$\kappa_S\cdot 10^6/\text{MPa}^{-1}$	$p_c/\text{MPa}\cdot\text{K}^{-1}$	$P_{\text{int}}/\text{MPa}$
<i>T</i> = 348 K									
390	2187.17	990.13	1829.24	1537.87	459.59	251.13	211.13	1.8301	237.72
0.1	1095.79	814.81	1868.79	1415.83	1196.16	1349.08	1022.09	0.8866	308.45
10	1158.06	825.02	1853.14	1421.98	1097.24	1177.84	903.80	0.9316	314.19
50	1355.91	857.43	1821.97	1438.96	870.62	803.22	634.37	1.0839	327.20
100	1539.68	887.26	1810.44	1459.72	726.13	589.66	475.43	1.2314	328.54
120	1601.92	897.29	1809.28	1467.49	686.93	535.45	434.30	1.2829	326.45
150	1686.98	910.91	1809.53	1478.63	639.44	472.08	385.75	1.3545	321.38
180	1764.17	923.20	1811.39	1489.23	601.49	423.33	348.04	1.4209	314.47
210	1835.13	934.43	1814.33	1499.36	570.27	384.53	317.78	1.4830	306.10
240	1900.99	944.81	1818.00	1509.06	544.01	352.84	292.88	1.5418	296.55
270	1962.61	954.48	1822.20	1518.40	521.53	326.42	272.00	1.5977	286.01
300	2020.61	963.54	1826.79	1527.40	502.01	304.02	254.20	1.6512	274.63
330	2075.49	972.08	1831.65	1536.10	484.86	284.76	238.81	1.7027	262.54
360	2127.65	980.17	1836.72	1544.53	469.64	268.01	225.37	1.7524	249.82
390	2177.41	987.86	1841.94	1552.71	456.02	253.29	213.51	1.8004	236.55
<i>T</i> = 363 K									
0.1	1035.38	800.04	1920.18	1461.78	1243.94	1531.61	1165.98	0.8122	294.72
10	1102.41	811.33	1900.91	1466.84	1129.21	1314.31	1014.19	0.8592	301.88
50	1310.60	846.26	1864.18	1483.57	875.80	864.43	687.94	1.0131	317.77
100	1500.42	877.67	1850.53	1504.10	722.19	622.68	506.11	1.1598	321.01
120	1564.25	888.11	1848.93	1511.82	681.29	562.78	460.17	1.2106	319.44
150	1651.22	902.25	1848.71	1522.91	632.14	493.46	406.50	1.2810	315.01
180	1729.93	914.95	1850.23	1533.47	593.14	440.65	365.21	1.3461	308.62

Table 8 (continued)

p/MPa	$c/(\text{m}\cdot\text{s}^{-1})^a$	$\rho/(\text{kg}\cdot\text{m}^{-3})$	$C_p/\text{J}\cdot\text{kg}^{-1}\cdot\text{K}^{-1}$	$C_p/\text{J}\cdot\text{kg}^{-1}\cdot\text{K}^{-1}$	$\alpha_p\cdot 10^6/\text{K}^{-1}$	$\kappa_T\cdot 10^6/\text{MPa}^{-1}$	$\kappa_S\cdot 10^6/\text{MPa}^{-1}$	$\rho_c/\text{MPa}\cdot\text{K}^{-1}$	$P_{\text{int}}/\text{MPa}$
210	1802.14	926.53	1852.91	1543.57	561.24	398.93	332.33	1.4069	300.69
240	1869.06	937.19	1856.39	1553.25	534.52	365.05	305.44	1.4642	291.51
270	1931.59	947.10	1860.43	1562.56	511.73	336.94	282.99	1.5187	281.30
300	1990.39	956.37	1864.88	1571.53	492.00	313.20	263.94	1.5709	270.22
330	2045.98	965.10	1869.62	1580.21	474.70	292.86	247.53	1.6209	258.39
360	2098.77	973.35	1874.59	1588.62	459.39	275.22	233.24	1.6692	245.91
390	2149.11	981.19	1879.71	1596.77	445.72	259.77	220.66	1.7159	232.86
<i>T</i> = 373 K									
0.1	995.62	790.01	1955.54	1492.73	1280.54	1672.88	1276.97	0.7655	285.42
10	1066.09	802.12	1933.51	1496.76	1153.63	1417.01	1096.93	0.8141	293.67
50	1281.41	838.86	1892.62	1513.32	880.06	907.96	726.00	0.9693	311.54
100	1475.20	871.36	1877.40	1533.64	720.02	645.56	527.35	1.1153	316.02
120	1540.07	882.10	1875.47	1541.30	677.96	581.60	477.97	1.1657	314.80
150	1628.29	896.58	1874.88	1552.31	627.66	508.09	420.67	1.2353	310.78
180	1707.99	909.56	1876.14	1562.81	587.95	452.43	376.87	1.2995	304.72
210	1781.01	921.36	1878.61	1572.85	555.58	408.68	342.17	1.3594	297.07
240	1848.62	932.22	1881.91	1582.47	528.55	373.29	313.90	1.4159	288.13
270	1911.74	942.29	1885.81	1591.73	505.55	344.02	290.37	1.4695	278.13
300	1971.06	951.70	1890.13	1600.66	485.67	319.37	270.46	1.5207	267.23
330	2027.11	960.56	1894.76	1609.29	468.28	298.29	253.35	1.5699	255.56
360	2080.32	968.92	1899.62	1617.65	452.91	280.05	238.48	1.6172	243.23
390	2131.02	976.85	1904.65	1625.75	439.20	264.09	225.42	1.6631	230.32
<i>T</i> = 383 K									
0.1	956.25	779.80	1991.89	1523.88	1321.65	1833.12	1402.42	0.7210	276.04

Table 8 (continued)

p/MPa	$c/(\text{m}\cdot\text{s}^{-1})^a$	$\rho/(\text{kg}\cdot\text{m}^{-3})$	$C_p/\text{J}\cdot\text{kg}^{-1}\cdot\text{K}^{-1}$	$C_p/\text{J}\cdot\text{kg}^{-1}\cdot\text{K}^{-1}$	$\alpha_p\cdot 10^6/\text{K}^{-1}$	$\kappa_T\cdot 10^6/\text{MPa}^{-1}$	$\kappa_S\cdot 10^6/\text{MPa}^{-1}$	$\rho_c/\text{MPa}\cdot\text{K}^{-1}$	$P_{\text{int}}/\text{MPa}$
10	1030.37	792.81	1966.78	1526.77	1180.67	1530.46	1188.06	0.7714	285.46
50	1252.98	831.50	1921.34	1543.10	885.01	953.81	766.04	0.9279	305.37
100	1450.73	865.12	1904.42	1563.12	718.24	669.15	549.23	1.0734	311.10
120	1516.62	876.15	1902.11	1570.69	674.97	600.91	496.21	1.1232	310.20
150	1606.06	891.00	1901.12	1581.60	623.51	523.01	435.11	1.1921	306.59
180	1686.73	904.26	1902.07	1592.00	583.07	464.41	388.70	1.2555	300.86
210	1760.55	916.29	1904.29	1601.95	550.23	418.56	352.11	1.3146	293.48
240	1828.83	927.33	1907.39	1611.50	522.88	381.62	322.42	1.3702	284.77
270	1892.53	937.57	1911.11	1620.68	499.66	351.16	297.79	1.4229	274.97
300	1952.36	947.13	1915.27	1629.53	479.64	325.57	277.00	1.4732	264.25
330	2008.86	956.10	1919.76	1638.08	462.15	303.74	259.18	1.5215	252.74
360	2062.48	964.57	1924.49	1646.36	446.71	284.89	243.72	1.5680	240.55
390	2113.55	972.61	1929.40	1654.39	432.96	268.42	230.16	1.6130	227.77
$T = 398 \text{ K}$									
10	977.92	778.65	2018.05	1572.06	1226.44	1723.88	1342.91	0.7114	273.15
50	1211.74	820.49	1964.98	1587.79	893.75	1027.25	830.06	0.8700	296.28
100	1415.36	855.87	1945.22	1607.20	716.32	705.92	583.26	1.0147	303.86
120	1482.75	867.36	1942.29	1614.60	671.19	630.83	524.40	1.0640	303.46
150	1573.98	882.75	1940.59	1625.28	617.92	545.97	457.26	1.1318	300.45
180	1656.06	896.44	1941.00	1635.48	576.36	482.73	406.75	1.1940	295.20
210	1731.05	908.82	1942.79	1645.23	542.79	433.61	367.20	1.2518	288.21
240	1800.32	920.16	1945.52	1654.59	514.96	394.26	335.30	1.3061	279.84
270	1864.87	930.64	1948.91	1663.59	491.41	361.96	308.97	1.3576	270.33
300	1925.45	940.41	1952.77	1672.27	471.16	334.94	286.83	1.4067	259.87

Table 8 (continued)

p/MPa	$c/(\text{m}\cdot\text{s}^{-1})^a$	$\rho/(\text{kg}\cdot\text{m}^{-3})$	$C_p/\text{J}\cdot\text{kg}^{-1}\cdot\text{K}^{-1}$	$C_p/\text{J}\cdot\text{kg}^{-1}\cdot\text{K}^{-1}$	$\alpha_p\cdot 10^6/\text{K}^{-1}$	$\kappa_T\cdot 10^6/\text{MPa}^{-1}$	$\kappa_s\cdot 10^6/\text{MPa}^{-1}$	$p_c/\text{MPa}\cdot\text{K}^{-1}$	$P_{\text{int}}/\text{MPa}$
<i>T</i> =403 K									
330	1982.62	949.57	1956.98	1680.65	453.52	311.96	267.91	1.4537	248.59
360	2036.84	958.21	1961.46	1688.76	437.98	292.17	251.55	1.4990	236.61
390	2088.46	966.39	1966.13	1696.63	424.16	274.93	237.25	1.5428	224.03
<i>T</i> =403 K									
10	960.73	773.87	2035.53	1587.27	1243.15	1795.37	1400.00	0.6924	269.05
50	1198.35	816.83	1979.67	1602.68	897.03	1053.04	852.51	0.8518	293.29
100	1403.91	852.82	1958.89	1621.85	715.89	718.56	594.93	0.9963	301.50
120	1471.80	864.46	1955.73	1629.18	670.11	641.06	534.02	1.0453	301.27
150	1563.61	880.04	1953.77	1639.76	616.23	553.78	464.78	1.1128	298.45
180	1646.16	893.87	1953.99	1649.87	574.29	488.94	412.84	1.1746	293.35
210	1721.53	906.37	1955.61	1659.54	540.48	438.70	372.28	1.2320	286.50
240	1791.12	917.80	1958.19	1668.82	512.48	398.52	339.63	1.2860	278.24
270	1855.95	928.37	1961.45	1677.74	488.82	365.60	312.71	1.3370	268.83
300	1916.77	938.21	1965.20	1686.34	468.49	338.08	290.11	1.3857	258.45
330	1974.16	947.43	1969.31	1694.65	450.79	314.72	270.82	1.4324	247.25
360	2028.58	956.12	1973.68	1702.69	435.21	294.61	254.16	1.4773	235.34
390	2080.38	964.35	1978.26	1710.49	421.37	277.10	239.60	1.5206	222.81
<i>T</i> =423 K									
10	893.40	754.37	2107.49	1648.78	1317.83	2122.90	1660.83	0.6208	252.58
50	1146.58	802.21	2039.14	1662.08	912.07	1163.32	948.21	0.7840	281.64
100	1359.78	840.72	2013.82	1680.02	715.25	771.11	643.29	0.9276	292.36
120	1429.60	853.01	2009.66	1686.98	666.81	683.33	573.61	0.9758	292.78
150	1523.71	869.33	2006.53	1697.07	610.39	585.81	495.46	1.0419	290.74
180	1608.07	883.75	2005.82	1706.72	566.89	514.27	437.58	1.1023	286.28

Table 8 (continued)

p/MPa	$c/(\text{m}\cdot\text{s}^{-1})^a$	$\rho/(\text{kg}\cdot\text{m}^{-3})$	$C_p/\text{J}\cdot\text{kg}^{-1}\cdot\text{K}^{-1}$	$C_p/\text{J}\cdot\text{kg}^{-1}\cdot\text{K}^{-1}$	$\alpha_p\cdot 10^6/\text{K}^{-1}$	$\kappa_T\cdot 10^6/\text{MPa}^{-1}$	$\kappa_S\cdot 10^6/\text{MPa}^{-1}$	$p_c/\text{MPa}\cdot\text{K}^{-1}$	$P_{\text{int}}/\text{MPa}$
210	1684.93	896.72	2006.68	1715.97	532.06	459.36	392.81	1.1583	279.95
240	1755.78	908.55	2008.59	1724.84	503.39	415.77	357.03	1.2107	272.14
270	1821.71	919.44	2011.25	1733.37	479.26	380.27	327.73	1.2603	263.11
300	1883.49	929.57	2014.45	1741.58	458.61	350.76	303.24	1.3075	253.07
330	1941.73	939.04	2018.04	1749.52	440.69	325.80	282.45	1.3527	242.17
360	1996.91	947.95	2021.93	1757.20	424.96	304.40	264.54	1.3961	230.54
390	2049.42	956.38	2026.05	1764.65	411.01	285.83	248.95	1.4380	218.26
$T=448\text{ K}$									
10	812.42	728.94	2202.17	1727.46	1430.59	2649.66	2078.49	0.5399	231.88
50	1085.71	783.90	2114.57	1735.31	935.49	1318.74	1082.22	0.7094	267.80
100	1308.21	825.81	2082.51	1751.05	717.04	841.51	707.57	0.8521	281.74
120	1380.34	838.92	2076.82	1757.36	665.04	739.33	625.61	0.8995	282.98
150	1477.20	856.22	2071.90	1766.56	605.25	627.74	535.23	0.9642	281.95
180	1563.73	871.39	2069.77	1775.40	559.70	547.13	469.31	1.0230	278.30
210	1642.37	884.97	2069.41	1783.88	523.55	485.98	418.92	1.0773	272.64
240	1714.72	897.29	2070.25	1792.01	493.99	437.89	379.03	1.1281	265.40
270	1781.94	908.61	2071.93	1799.84	469.25	399.01	346.61	1.1760	256.87
300	1844.86	919.09	2074.23	1807.37	448.17	366.88	319.68	1.2216	247.26
330	1904.12	928.88	2076.98	1814.65	429.94	339.85	296.93	1.2651	236.75
360	1960.22	938.06	2080.07	1821.69	413.98	316.78	277.43	1.3068	225.47
390	2013.55	946.73	2083.42	1828.52	399.88	296.84	260.52	1.3471	213.50
$T=473\text{ K}$									
10	734.98	702.03	2301.72	1808.03	1568.35	3356.89	2636.88	0.4672	210.99
50	1028.95	765.47	2189.72	1805.59	964.49	1496.41	1233.91	0.6445	254.86

Table 8 (continued)

p/MPa	$c/(\text{m}\cdot\text{s}^{-1})^a$	$\rho/(\text{kg}\cdot\text{m}^{-3})$	$C_p/\text{J}\cdot\text{kg}^{-1}\cdot\text{K}^{-1}$	$C_p/\text{J}\cdot\text{kg}^{-1}\cdot\text{K}^{-1}$	$\alpha_p\cdot 10^6/\text{K}^{-1}$	$\kappa_T\cdot 10^6/\text{MPa}^{-1}$	$\kappa_S\cdot 10^6/\text{MPa}^{-1}$	$\rho_c/\text{MPa}\cdot\text{K}^{-1}$	P_{int}/MPa
100	1260.40	811.05	2149.52	1818.26	721.92	917.53	776.13	0.7868	272.16
120	1334.74	825.05	2141.97	1823.67	666.07	799.09	680.35	0.8335	274.26
150	1434.18	843.35	2134.86	1831.66	602.69	671.90	576.47	0.8970	274.28
180	1522.76	859.30	2130.95	1839.38	554.95	581.43	501.87	0.9545	271.46
210	1603.06	873.49	2129.06	1846.81	517.39	513.58	445.49	1.0074	266.51
240	1676.83	886.32	2128.54	1853.94	486.88	460.70	401.27	1.0568	259.88
270	1745.26	898.06	2128.98	1860.80	461.48	418.26	365.57	1.1033	251.88
300	1809.24	908.91	2130.11	1867.41	439.93	383.40	336.11	1.1475	242.75
330	1869.44	919.01	2131.77	1873.79	421.36	354.22	311.35	1.1896	232.66
360	1926.39	928.48	2133.83	1879.97	405.15	329.42	290.23	1.2299	221.75
390	1980.49	937.39	2136.20	1885.97	390.86	308.06	271.98	1.2687	210.12

Relative expanded uncertainties ($k=2$) at 95% confidence of: density, $U(\rho)=0.2\%$; isobaric specific heat capacity, $U(C_p)=2.2\%$; isochoric specific heat capacity, $U(C_v)=2.6\%$; isobaric expansivity, $U(\alpha_p)=1\%$; isothermal compressibility, $U(\kappa_T)=0.6\%$; isentropic compressibility, $U(\kappa_S)=0.2\%$; thermal pressure coefficient, $U(\rho_c)=1\%$; internal pressure, $U(p_{int})=2.7\%$. ^aSound-speed values calculated using correlations from Eqs. 1 and 2

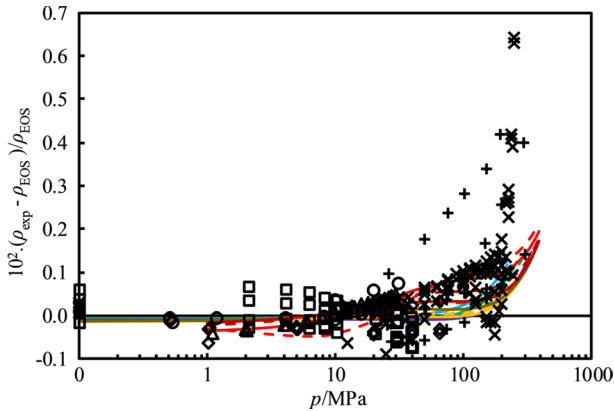


Fig. 7 Deviations from the Helmholtz EOS of Lemmon and Span [4] of liquid densities of toluene, ρ_{exp} , as a function of pressure at various temperatures. Derived in this work ($u(\rho)=0.20\%$, $k=2$) (solid and dotted lines): —, $T=283$ K; - - -, $T=298$ K; — · —, $T=306$ K; - · - · -, $T=321$ K; — · — · —, $T=343$ K; — · — · — · —, $T=348$ K; — · — · — · — · —, $T=363$ K; — · — · — · — · — · —, $T=373$ K; — · — · — · — · — · — · —, $T=383$ K; — · — · — · — · — · — · — · —, $T=398$ K; — · — · — · — · — · — · — · — · —, $T=403$ K; — · — · — · — · — · — · — · — · — · —, $T=423$ K; — · — · — · — · — · — · — · — · — · — · —, $T=448$ K; — · — · — · — · — · — · — · — · — · — · — · —, $T=473$ K. Literature data (experimental): \square , Moravkova et al. [33] from 298.15 K to 328.15 K; Δ , Sommer et al. [3] at 453.15 K and 473.15 K; \times , Kashiwagi et al. [34] between 273.15 K and 373.12 K; $+$, Dymond et al. [35] between 298.23 K and 373.27 K; \circ , McLinden and Splett [25] between 283.15 K and 473.16 K; \diamond , Tay and Trusler [21] between 283.16 K and 473.15 K

7 Comparison of Derived Properties with Literature Data

The derived density ρ , isobaric heat capacity C_p , isobaric expansivity α_p , isothermal compressibility κ_T and isochoric heat capacity C_v obtained by means of thermodynamic integration and relations described in the previous section were compared against the values obtained from Helmholtz EOS of Lemmon and Span [4] and literature data, with the EOS as the baseline. Although there are a great amount of experimental data available for density of liquid toluene in our temperature and pressure range, experimental data of other thermodynamic properties are limited. Therefore, comparisons against the derived thermodynamic properties data reported in literature are also provided where necessary.

All comparisons are made at isotherms near the average experimental temperatures as functions of pressure. Figure 7 shows the relative percentage deviation of derived density and literature data against the EOS. The deviations increase with increasing temperature with the lowest deviations observed at the lowest pressures. Most of our derived density values lie within the reported uncertainty of 0.05% of the EOS up to 100 MPa and within the reported uncertainty of 0.5% of the EOS at higher pressures. Average deviations of our data against the EOS are $\Delta_{\text{AARD}}=0.05\%$ with maximum deviation, $\Delta_{\text{MARD}}=0.2\%$ over the entire pressure range. These results suggest very close agreement between our derived data and the EOS prediction for density, mainly due to the high-quality fits of sound speed and density at reference isobar.

The deviations in density of Kashiwagi et al. [34] between $T=(273.15$ and $373.14)$ K and $p=(0.1$ and $250)$ MPa are up to 0.6% from the EOS. The data of

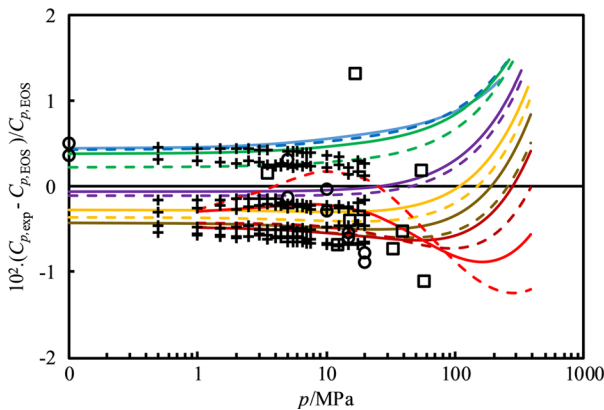


Fig. 8 Deviations from the Helmholtz EOS of Lemmon and Span [4] of liquid isobaric heat capacities of toluene, $C_{p,\text{exp}}$, as a function of pressure at various temperatures. Derived in this work ($u(C_p)=2.2\%$, $k=2$) (solid and dotted lines): —, $T=283$ K; - - - , $T=298$ K; — · — , $T=306$ K; - · - · , $T=321$ K; - · - · , $T=343$ K; - · - · , $T=348$ K; - · - · , $T=363$ K; - · - · , $T=373$ K; - · - · , $T=383$ K; - · - · , $T=398$ K; - · - · , $T=403$ K; - · - · , $T=423$ K; - · - · , $T=448$ K; - · - · , $T=473$ K. Literature data (experimental): □, Shulga et al. [36] at 326.20 K, 354.50 K and 401.50 K; +, Akhundov and Eksaev [26] between 298.14 K to 473.11 K; ○, Segovia et al. [37] at 313.15 K and 333.15 K

Dymond et al. [35] between temperatures of 298.23 K to 373.27 K and pressures up to 300 MPa are at a maximum of 0.4%. More recent data of Morávková et al. ($T=(273.15$ to $373.14)$ K and $p=(0.1$ to $250)$ MPa) [33], McLinden & Splett [25], Sommer et al. [3] and Tay & Trusler [21] show better agreement with the EOS with maximum deviations in the experimental range of this work of 0.08%, 0.07%, 0.05% and 0.06%, respectively.

Similarly, the derived isobaric heat capacity is compared against the EOS and available experimental and derived data from the literature as shown in Fig. 8. The derived values are in close agreement with the EOS with $\Delta_{\text{AARD}}=0.5\%$ and $\Delta_{\text{MARD}}=1.5\%$. The highest deviations generally occur at the highest pressures and lowest temperatures. All derived values fall within the reported experimental uncertainty of the EOS, which are reported to be up to 3%. The experimental data of Shulga et al. [36] at $T=(326.20, 354.50$ and $401.50)$ K and pressures up to 54 MPa deviate up to 1.3% from the EOS. Similarly, the data of Akhundov et al. [26] between 298.14 K and 473.11 K and pressures up to 20 MPa vary from the EOS by up to 0.7%. The data of Segovia et al. [37] at 313.15 K and 333.15 K and pressures up to 30 MPa vary from the EOS by up to 0.9%.

Our derived isobaric expansivity values compared against the EOS indicate maximum deviations of nearly 3% occurring at the lowest pressures of the highest temperatures as shown in Fig. 9. The experimental data for isobaric expansivity of liquid toluene of Chorazewski et al. [38] between $T=(304.1$ and $422.2)$ K and pressures up to 195 MPa deviate from the EOS by as much as 8.6%. The experimental data of Navia et al. [39] between $T=(308.15$ and $348.15)$ K and pressures up to 55 MPa are in much closer agreement with the EOS. The average

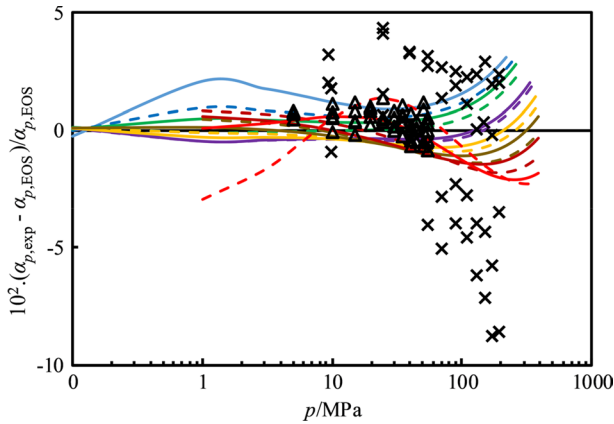


Fig. 9 Deviations from the Helmholtz EOS of Lemmon and Span [4] of liquid isobaric expansivities of toluene, $\alpha_{p,exp}$, as a function of pressure at various temperatures. Derived in this work ($u(\alpha_p)=0.60\%$, $k=2$) (solid and dotted lines): —, $T=283$ K; —•—, $T=298$ K; —▲—, $T=306$ K; —■—, $T=321$ K; —□—, $T=343$ K; —◇—, $T=348$ K; —○—, $T=363$ K; —△—, $T=373$ K; —▽—, $T=383$ K; —◇—, $T=398$ K; —○—, $T=403$ K; —△—, $T=423$ K; —◇—, $T=448$ K; —○—, $T=473$ K. Literature data (experimental): ×, Chorazewski et al. [38] between $T=(304.1$ and $422.2)$ K; Δ, Navia et al. [39] between $T=(308.15$ and $348.15)$ K

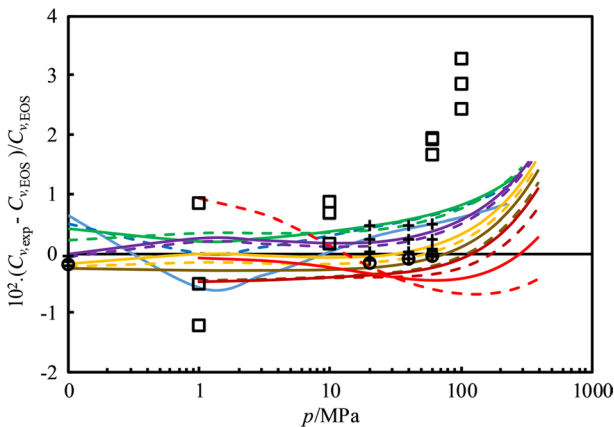


Fig. 10 Deviations from the Helmholtz EOS of Lemmon and Span [4] of liquid isochoric heat capacities of toluene, $C_{v,exp}$, as a function of pressure at various temperatures. Derived in this work ($u(C_v)=2.6\%$, $k=2$) (solid lines): —, $T=283$ K; —•—, $T=298$ K; —▲—, $T=306$ K; —■—, $T=321$ K; —□—, $T=343$ K; —◇—, $T=348$ K; —○—, $T=363$ K; —△—, $T=373$ K; —▽—, $T=383$ K; —◇—, $T=398$ K; —○—, $T=403$ K; —△—, $T=423$ K; —◇—, $T=448$ K; —○—, $T=473$ K. Literature data (all reported as derived values): □, EOS of Goodwin [23] at 320 K, 400 K and 470 K; ○, Sun et al. [40] at 320 K; +, Shchamialiou et al. [19] between $T=(313.15$ and $413.15)$ K

deviations of their data are nearly 0.5% with maximum deviations of 1.4%. Both these experimental datasets have reported uncertainty of 2%.

Figure 10 shows comparison between our derived isochoric heat capacity values against the EOS with $\Delta_{AARD}=0.5\%$ and $\Delta_{MARD}=1.5\%$. Experimental data of isochoric heat capacity values for our range of study are not currently available in the literature.

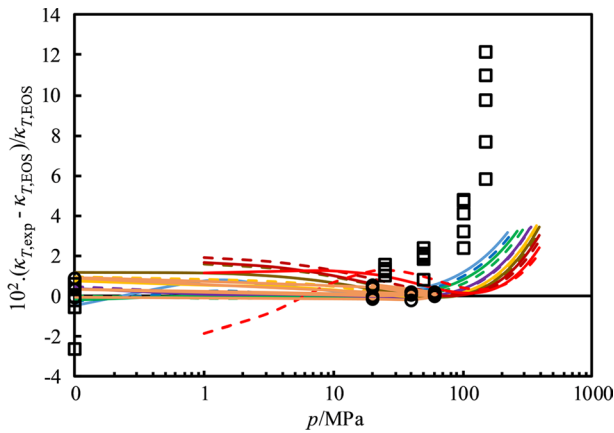


Fig. 11 Deviations from the Helmholtz EOS of Lemmon and Span [4] of liquid isothermal compressibilities of toluene, $\kappa_{T,\text{exp}}$, as a function of pressure at various temperatures. Derived in this work ($u(\kappa_T)=0.28\%$, $k=2$) (solid and dotted lines): —, $T=283$ K; —, $T=298$ K; —, $T=306$ K; —, $T=321$ K; —, $T=343$ K; —, $T=348$ K; —, $T=363$ K; —, $T=373$ K; —, $T=383$ K; —, $T=398$ K; —, $T=403$ K; —, $T=423$ K; —, $T=448$ K; —, $T=473$ K. Literature data (all reported as derived values): \square , Eastel et al. [41] between $T=(278.15$ and $323.14)$ K; \circ , Shchamialiou et al. [19] between $T=(313.15$ and $413.15)$ K

Therefore, comparisons of derived values from the literature against the EOS are provided. The deviations of values obtained from non-analytical EOS of Goodwin [23] against the Helmholtz EOS at $T=(320, 400$ and $470)$ K and at pressures up to 100 MPa are up to 3% with the highest deviations occurring at highest pressures. Similarly, the derived data of Sun et al. [40] obtained from sound-speed data at 320 K and pressures up to 60 MPa show maximum deviations of up to 0.17%. At that temperature and pressure range, our data indicate maximum deviations of nearly 0.3% against the Helmholtz EOS. The derived data of Shchamialiou et al. [19] between $T=(313.15$ and $413.15)$ K and pressures up to 60 MPa vary by up to 0.5% from the EOS.

In addition, the derived isothermal compressibility values of liquid toluene are compared against the Helmholtz EOS as shown in Fig. 11. Deviations from the EOS of our derived data are $\Delta_{\text{AARD}}=1\%$ and $\Delta_{\text{MARD}}=3.5\%$. Derived values of isothermal compressibility available in the literature are also compared against the EOS. The data of Eastel et al. [41] between $T=(278.15$ and $323.14)$ K at pressures up to 275 MPa show very high deviations of up to 44% when compared to the EOS. These very high deviations occur at the highest pressures. For clarity, the highest deviations of this dataset are not included in Fig. 11. The derived isothermal compressibility of Shchamialiou et al. [19] between $T=(313.15$ and $413.15)$ K and pressures up to 60 MPa varies by up to 0.9% from the EOS.

8 Conclusions

Accurate measurements of the speed-of-sound liquid toluene in the temperature range between 283.15 K and 473.15 K were carried out at pressures up to 390 MPa using double-path pulse-echo method independently at UWA and ICL. A comparison of the resulting data with the most accurate literature data available to date along with three different EOS was carried out. The standard uncertainties of our experimental data are at most 0.06%, which fall well within the reported EOS uncertainty of 2%. Comparison with recent and most accurate literature data shows good agreement, with maximum deviations of up to 0.08%. By employing the method of thermodynamic integration, a range of thermodynamic properties were derived and compared against the existing literature experimental and derived data as well as the Helmholtz EOS. Our derived properties show better agreement with the EOS within the range of uncertainties as compared to the most experimental and derived properties. In addition, a comprehensive error propagation analysis was carried out, and uncertainties of derived properties were evaluated empirically using a method previously employed for pure water. Temperature derivatives of perturbations were evaluated by employing sum-of-sine fit to capture accurate dynamic fluctuations of the perturbations in derived properties. Finally, we suggest that the highly accurate sound-speed measurements, along with derived properties obtained here and recent literature data, could potentially be used to improve the Helmholtz EOS for toluene.

Supplementary Information The online version contains supplementary material available at <https://doi.org/10.1007/s10765-021-02917-7>.

Acknowledgements This work was funded by the Australian Research Council through DP190103538. The authors thank Jonathan Choong for assistance developing parts of the analysis code.

Declarations

Conflict of interest There are no relevant financial or non-financial conflicts of interest or competing interests to report.

Data Availability N/A.

Code availability N/A.

Ethical Approval N/A.

Consent to Participate N/A.

Consent for Publication N/A.

References

1. M.J. Assael et al., Reference correlation of the thermal conductivity of toluene from the triple point to 1000 K and up to 1000 MPa. *J. Phys. Chem. Ref. Data* **41**(2), 023101–023101 (2012)
2. H. Ziebland, The thermal conductivity of toluene. New determinations and an appraisal of recent experimental work. *Int. J. Heat Mass Transf.* **2**(4), 273–279 (1961)
3. D. Sommer et al., Measurement and correlation of the (p, ρ, T) relation of liquid cyclohexane, toluene, and ethanol in the temperature range from 23315 K to 47315 K at pressures up to 30 MPa for use as density reference liquids. *J. Chem. Thermodyn.* **43**(2), 117–132 (2011)
4. E.W. Lemmon, R. Span, Short fundamental equations of state for 20 industrial fluids. *J. Chem. Eng. Data* **51**(3), 785–850 (2006)
5. E.B. Freyer, J.C. Hubbard, D.H. Andrews, Sonic studies of the physical properties of liquids. I. The sonic interferometer. The velocity of sound in some organic liquids and their compressibilities I. *J. Am. Chem. Soc.* **51**(3), 759–770 (1929)
6. D.D. Deshpande, L.G. Bhatgadde, Sound velocities, adiabatic compressibilities, and free volumes in aniline solutions. *J. Phys. Chem.* **72**(1), 261–266 (1968)
7. V.V. Zotov, Y.A. Neruchev, N.F. Otpushchennikov, Measurement of the velocity of sound in toluene at the saturation line. *Sov. Phys. J.* **12**(2), 252–253 (1969)
8. S. Reddy, Isentropic compressibilities of binary liquid mixtures at 303.15 and 313.15 K. *J. Chem. Eng. Data* **31**(2), 238–240 (1986)
9. K. Tamura, S. Murakami, S. Doi, Speeds of sound, densities, and isentropic compressibilities of $\{x\text{-C}_6\text{H}_{12} + (1 - x) \text{C}_6\text{H}_5\text{CH}_3\}$, $\{x\text{-C}_6\text{H}_{11}\text{CH}_3 + (1 - x) \text{C}_6\text{H}_6\}$, and $\{x\text{-C}_6\text{H}_{11}\text{CH}_3 + (1 - x) \text{C}_6\text{H}_5\text{CH}_3\}$, from 293.15 to 303.15 K. *J. Chem. Thermodyn.* **17**(4), 325–333 (1985)
10. R. Gonzalez-Olmos et al., Influence of temperature on thermodynamic properties of methyl *t*-butyl ether (MTBE) + gasoline additives. *Int. J. Thermophys.* **28**(4), 1199–1227 (2007)
11. D.J. Luning Prak et al., Viscosity, speed of sound, bulk modulus, surface tension, and flash point of binary mixtures of *n*-hexadecane + ethyl benzene or + toluene at (293.15 to 373.15) K and 0.1 MPa. *J. Chem. Eng. Data* **59**(11), 3571–3585 (2014)
12. D. Dragoescu, F. Sirbu, A. Shchamialiou, Thermodynamic properties for binary mixtures of 1-chlorohexane + some hydrocarbons at different temperatures and atmospheric pressure. *J. Mol. Liq.* **294**, 111510 (2019)
13. T. Takagi, H. Teranishi, Ultrasonic speeds and thermodynamics for (toluene+ *o*-xylene) and (toluene+ aniline) under high pressures. *J. Chem. Thermodyn.* **17**(11), 1057–1062 (1985)
14. M.J.P. Muringer, N.J. Trapeniers, S.N. Biswas, The effect of pressure on the sound velocity and density of toluene and *n*-heptane up to 2600 bar. *Phys. Chem. Liq.* **14**(4), 273–296 (1985)
15. V.S. Okhotin et al., Sound velocity in liquid toluene. *Teplotfiz. Svoystva Veshchestv Mater.* **24**, 5–13 (1988)
16. V.N. Verveiko, G.A. Melnikov, Y.F. Melikhov, Acoustic and P-V-T study of halogenated benzenes and toluenes in a wide range of temperatures and pressures (to 600 MPa). *Teplotfiz. Svoystva Veshchestv Mater.* **30**, 5–16 (1991)
17. K. Meier, S. Kabelac, Measurements of the Speed of Sound in Liquid Toluene. *J. Chem. Eng. Data* **58**(5), 1398–1406 (2013)
18. F. Yebra, J. Troncoso, L. Romaní, Fully automatized apparatus for determining speed of sound for liquids in the temperature and pressure interval (283.15–343.15) K and (0.1–95) MPa. *J. Chem. Thermodyn.* **104**, 102–109 (2017)
19. A.P. Shchamialiou et al., Densities, speed of sound, and derived thermodynamic properties of toluene, tetradecane, and 1-chlorohexane in the compressed liquid region. *Fluid Phase Equilib.* **507**, 112427 (2020)
20. S.Z.S. Al Ghafri et al., Speed of sound and derived thermodynamic properties of para-xylene at temperatures between (306 and 448) K and at pressures up to 66 MPa. *J. Chem. Thermodyn.* **135**, 369–381 (2019)
21. W.J. Tay, J.P.M. Trusler, Density, sound speed and derived thermophysical properties of *n*-nonane at temperatures between (283.15 and 473.15) K and at pressures up to 390 MPa. *J. Chem. Thermodyn.* **124**, 107–122 (2018)
22. A. Polt, B. Platzler, G. Maurer, Parameter der thermischen Zustandsgleichung von Bender fuer 14 mehratomige reine Stoffe. *Chem. Tech. (Leipzig)* **44**(6), 216–224 (1992)

23. R.D. Goodwin, Toluene thermophysical properties from 178 to 800 K at pressures to 1000 bar. *J. Phys. Chem. Ref. Data* **18**(4), 1565–1636 (1989)
24. M. Trusler, *Physical Acoustics and Metrology of Fluids* (CRC Press, Boca Raton, 1991)
25. M.O. McLinden, J.D. Splett, A liquid density standard over wide ranges of temperature and pressure based on toluene. *J. Res. Natl Inst. Stand. Technol.* **113**, 29–67 (2008)
26. T.S.E. Akhundov, R.A. Mustafaev, Experimental determination of the isobaric specific heat of toluene in supercritical and vapor regions. *Izv. Vyssh. Uchebn. Zaved., Neft Gaz.* **16**(3), 68 (1973)
27. R.D. Chirico, W.V. Steele, Reconciliation of calorimetrically and spectroscopically derived thermodynamic properties at pressures greater than 0.1 MPa for benzene and methylbenzene: the importance of the third virial coefficient. *Ind. Eng. Chem. Res.* **33**(1), 157–167 (1994)
28. C.A. Cerdeiriña et al., temperature dependence of the excess molar heat capacities for alcohol–alkane mixtures. Experimental testing of the predictions from a two-state model. *J. Phys. Chem. B* **106**(1), 185–191 (2002)
29. M.J. Pedersen, W.B. Kay, H.C. Hershey, Excess enthalpies, heat capacities, and excess heat capacities as a function of temperature in liquid mixtures of ethanol + toluene, ethanol + hexamethyldisiloxane, and hexamethyldisiloxane + toluene. *J. Chem. Thermodyn.* **7**(12), 1107–1118 (1975)
30. M.J. Dávila, J.P. Martin-Trusler, Thermodynamic properties of mixtures of N-methyl-2-pyrrolidone and methanol at temperatures between 298.15 K and 343.15 K and pressures up to 60 MPa. *J. Chem. Thermodyn.* **41**(1), 35–45 (2009)
31. J.P.M. Trusler, E.W. Lemmon, Determination of the thermodynamic properties of water from the speed of sound. *J. Chem. Thermodyn.* **109**, 61–70 (2017)
32. K.F. Herzfeld, T.A. Litovitz, *Absorption and Dispersion of Ultrasonic Waves*, vol. 7 (Academic Press, New York, 2013)
33. L. Morávková, Z. Wagner, J. Linek, (P, Vm, T) Measurements of (toluene+ propiophenone) at temperatures from 298.15 K to 328.15 K and at pressures up to 40 MPa. *J. Chem. Thermodyn.* **37**(7), 658–666 (2005)
34. H. Kashiwagi et al., Thermal conductivity and density of toluene in the temperature range 273–373 K at pressures up to 250 MPa. *Int. J. Thermophys.* **3**(3), 201–215 (1982)
35. J.H. Dymond et al., Transport properties of nonelectrolyte liquid mixtures VIII Viscosity coefficients for toluene and for three mixtures of toluene + hexane from 25 to 100°C at pressures up to 500 MPa. *Int. J. Thermophys.* **12**, 275–287 (1991)
36. V.M. Shulga et al., Thermal conductivity and heat capacity of liquid toluene at temperatures between 255 and 400 K and at pressures up to 1000 MPa. *Int. J. Thermophys.* **7**(6), 1147–1161 (1986)
37. J.J. Segovia et al., High-pressure isobaric heat capacities using a new flow calorimeter. *J. Supercrit. Fluids* **46**(3), 258–264 (2008)
38. M. Chorazewski, J.-P.E. Grolier, S.L. Randzio, Isobaric thermal expansivities of toluene measured by scanning transitiometry at temperatures from (243 to 423) K and pressures up to 200 MPa. *J. Chem. Eng. Data* **55**(12), 5489–5496 (2010)
39. P. Navia, J. Troncoso, L. Romání, New calibration methodology for calorimetric determination of isobaric thermal expansivity of liquids as a function of temperature and pressure. *J. Chem. Thermodyn.* **40**(11), 1607–1611 (2008)
40. T.F. Sun et al., Evaluation of the thermophysical properties of toluene and n-heptane from 180 to 320 K and up to 260 MPa from speed-of-sound data. *Ber. Bunsenges. Phys. Chem.* **95**(6), 696–704 (1991)
41. A.J. Easteal, L.A. Woolf, p, V, T and derived thermodynamic data for toluene, trichloromethane, dichloromethane, acetonitrile, aniline, and n-dodecane. *Int. J. Thermophys.* **6**(4), 331–351 (1985)

Authors and Affiliations

Subash Dhakal¹ · Weparn J. Tay² · Saif Z. S. Al Ghafri¹ · Darren Rowland¹ · Sean P. Mullins¹ · Eric F. May¹ · J. P. Martin Trusler² · Paul L. Stanwix¹ 

¹ Fluid Science & Resources Division, Department of Chemical Engineering, The University of Western Australia, Crawley, WA 6009, Australia

² Department of Chemical Engineering, Imperial College London, London SW7 2AZ, UK